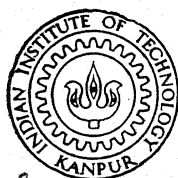
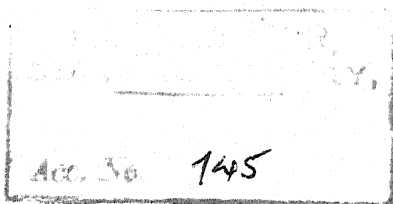


MÖSSBAUER STUDIES OF LEADZIRCONATE-TITANATE-STANNATE

By
VEERAVANALLUR SRINIVASAN SUNDARAM



ME-1968-M-SUN-MOS.

Thesis
669.4
Su 72 m

DEPARTMENT OF METALLURGICAL ENGINEERING
INDIAN INSTITUTE OF TECHNOLOGY KANPUR

December, 1968

MÖSSBAUER STUDIES OF LEAD ZIRCONATE-TITANATE-STANNATE

A thesis submitted

In partial fulfilment of the requirements

for the Degree of

MASTER OF TECHNOLOGY

by

VEERAVANALLUR SRINIVASAN SUNDARAM

to the

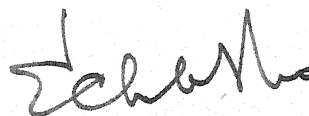
Department of Metallurgical Engineering

Indian Institute of Technology, Kanpur

December 1968

CERTIFICATE

Certified that this work on "Mössbauer
Studies of Lead Zirconate-Titanate-Stannate" by
V.S. Sundaram has been carried out under my supervision
and that this has not been submitted elsewhere for a degree .



Dr. E.C. Subba Rao
Professor

Department of Metallurgical Engineering
Indian Institute of Technology, Kanpur.

ACKNOWLEDGEMENTS

I am very much grateful to Professor E.C. Subbarao under whose supervision and able guidance I have been able to work in this new branch, namely, Ferroelectricity and Mössbauer Effect.

I would like to record my gratitude to Professor C.R. Kanekar of the Tata Institute of Fundamental Research, Bombay for allowing me to use his set up and for his keen interest in the work.

I am indebted to Dr. Bernard Jaffe of Clevite Corporation, U.S.A. for supplying the sample used in the present study and for communicating some of his unpublished data relating to the same material.

I am very much thankful to Professor K.P. Gupta, Head of the Department of Metallurgical Engineering, IIT-Kanpur for his critical suggestions in the design of the vacuum furnace and to Mr. V.P. Gupta for his excellent fabrication of the furnace.

I would like to express my hearty thanks to Shri K.R.P.M. Rao and Dr. V.U.S. Rao of T.I.F.R., Bombay for their help during the Mössbauer Effect studies. Thanks are also due to Dr. R.N. Patil for his helpful discussions and to Messrs. S. Krishnamoorthy of the Dielectrics Laboratory and T.S. Radhakrishnan of T.I.F.R., Bombay for their help at various stages of the work.

Finally, thanks are also due to Mr. M. Natu for his excellent typing, and my numerous friends in the Dielectric Materials group.

TABLE OF CONTENTS

CHAPTER		Page
	LIST OF TABLES	vi
	LIST OF FIGURES	vii
	SYNOPSIS	viii
I	- FERROELECTRICITY AND ANTIFERROELECTRICITY	1
	1.2 Antiferroelectrics	2
	1.3 Criteria of Ferroelectricity	3
	1.3.1 Dielectric Hysteresis	4
	1.3.2 Dielectric Constant	4
	1.3.3 Other Considerations	7
	1.4 Theory of Ferro- Antiferro- Electricity	7
	1.4.1 Phenomenological Theory	9
	1.4.2 Devonshire-Slater Theory of BaTiO_3	13
	1.4.3 Lattice Dynamical Theory	16
II	- MÖSSBAUER EFFECT	22
	2.1 Classical Approach	25
	2.2 Conditions for the Mössbauer Effect	30
	2.3 Isomer Shift	30
	2.4 Quadrupole Coupling	32
	2.5 Mössbauer Effect and Ferroelectricity	36
III	- LEAD ZIRCONATE AND ITS MODIFIED COMPOUNDS	41
IV	- PURPOSE OF THE PRESENT WORK	45

V - EXPERIMENTAL

46

5.1 Sample Preparation

46

5.2 Thermal Expansion Measurements

46

5.3 Dielectric Measurements

48

5.4 Hysteresis Measurements

48

5.5 Mössbauer Effect Measurements

51

5.5.1 Furnace Assembly

53

5.5.2 Curve Fitting

55

VI - RESULTS AND DISCUSSIONS

63

6.1 Quadrupole Splitting

63

6.2 Isomer Shift

66

6.3 Mössbauer Line Intensities

67

BIBLIOGRAPHY

74

LIST OF TABLES

	Page
TABLE 1 - VALUES OF DIELECTRIC CONSTANT AT DIFFERENT TEMPERATURES	71
TABLE 2 - ISOMER SHIFT AND HALF WIDTH VALUES AT DIFFERENT TEMPERATURES	72
TABLE 3 - MOSSBAUER LINE INTENSITY AT DIFFERENT TEMPERATURES (NORMALISED TO THE ROOM TEMPERATURE VALUE)	73

LIST OF FIGURES

	Page
FIG. 1 - WIRING DIAGRAM OF THE FERROELECTRIC ANALYSER	5
FIG. 2 - COMPOSITION-TEMPERATURE PHASE DIAGRAM - $\text{Pb}_{.99}\text{Nb}_{.02}((\text{Zr}_{.5}\text{Sn}_{.5})_{1-y}\text{Ti}_y)_{.98}\text{O}_3$	44
FIG. 3 - LINEAR THERMAL EXPANSION OF $\text{Pb}_{.99}\text{Nb}_{.02}((\text{Zr}_{.5}\text{Sn}_{.5})_{.88}\text{Ti}_{.12})_{.98}\text{O}_3$ (UNPOLED SAMPLE)	47
FIG. 4 - VARIATION OF DIELECTRIC CONSTANT WITH TEMPERATURE	49
FIG. 5 - FERROELECTRIC-ANTIFERROELECTRIC HYSTERESIS LOOPS	50
FIG. 6 - BLOCK DIAGRAM OF THE MÖSSBAUER SET UP	52
FIG. 7 - VACUUM FURNACE ASSEMBLY	54
FIG. 8 - THE MÖSSBAUER SPECTRUM AT 25° C	56
FIG. 9 - THE MÖSSBAUER SPECTRA AT 60° AND 85° C	57
FIG. 10 - THE MÖSSBAUER SPECTRA AT 90° C AND 95° C	58
FIG. 11 - THE MÖSSBAUER SPECTRA AT 100° C AND 110° C	59
FIG. 12 - THE MÖSSBAUER SPECTRA AT 115° C AND 120° C	60
FIG. 13 - THE MÖSSBAUER SPECTRA AT 125° C AND 165° C	61
FIG. 14 - VARIATION OF THE MÖSSBAUER LINE INTENSITY WITH TEMPERATURE	69

SYNOPSIS

MÖSSBAUER STUDIES IN LEAD ZIRCONATE-TITANATE-STANNATE

A thesis submitted

by

Veeravanallur Srinivasan Sundaram

to the

Department of Metallurgical Engineering
 Indian Institute of Technology, Kanpur
 for the Degree of M.Tech. in Dec. 1968.

The present work is concerned with the study of the Mössbauer Effect in Lead Zirconate-Titanate-Stannate. The compound studied is $\text{Pb}_{.99}\text{Nb}_{.02} \left\{ (\text{Zr}_{.5}\text{Sn}_{.5})_{.88} \text{Ti}_{.12} \right\}_{.98} \text{O}_3$, which exhibits the following sequence of transitions- namely, ferroelectric (rhombohedral) to antiferroelectric (tetragonal multiple cell) at 95°C , antiferroelectric to paraelectric (multiple cubic) at 120°C and paraelectric (multiple cubic) to paraelectric (simple cubic) at 150°C . The transition temperatures given above were confirmed by dielectric constant and hysteresis loop measurements at different temperatures. Using a loud speaker driven constant velocity unit the Mössbauer Effect measurements were carried out. From the observed spectra at different temperatures, the variation of the Mössbauer parameters such as isomer shift, line intensity, etc. with temperature were found. The anomalies in the Mössbauer line intensity around the two transition temperatures are discussed in the light of W. Cochran's theory of ferroelectricity and B.D. Silverman's Linear Chain model of antiferroelectricity.

CHAPTER - I

FERROELECTRICITY AND ANTIFERROELECTRICITY

A ferroelectric is, by definition, a crystalline solid that has two properties. Firstly it belongs to a crystal point group that is polar and secondly the polarity can be reversed without destroying the crystal. Normally the polarity is reversed by applying an electric field so that in an alternating field hysteresis loops are obtained, but in at least one ferroelectric, sodium ammonium tartrate the polarity can be reversed only by applying a suitable stress (Takagi et al (1)).

Of the twentyone noncentrosymmetric crystal classes, except the cubic crystal class 432, the remaining are piezoelectric. Ten of these twenty piezoelectric classes are characterised by a unique polar axis. Crystals in these classes are called polar because they are spontaneously polarised. These ten classes are also pyroelectric. Thus the ferroelectric crystals belong to the pyroelectric family. However, they constitute only that part for which the direction of spontaneous polarisation can be reversed by the application of an electric field. Thus a ferroelectric crystal is a pyroelectric crystal with a reversible polarisation.

Since the atomic shifts produced by an electric field can only be small, it follows that the two states with opposite polarity will differ only slightly from each other and hence a half way nonpolar state exists. This means there is a nonpolar state, only slightly unstable, so that raising the temperature will change the relative stabilities such that, the material at some temperature will transform to nonpolar state. In fact most ferroelectrics have a Curie temperature above which they are

nonpolar; however, this is not an essential feature - for a number of ferroelectrics are known which decompose before the Curie temperature is attained, e.g., Lithium trihydrogen selenite (Pepinsky et al(2)).

The ferroelectrics may be simple compounds such as BaTiO_3 or complex ones such as Rochelle salt. They may have a great variety of crystal symmetry. The forces between the constituent ions may be largely ionic or covalent or even intermolecular. The onset of polarity may be due to ordering of dipoles that already exist in the structure or to the creation of new dipoles by ionic shifts. Merz(3) classifies the ferroelectrics as hard and soft ferroelectrics. The hard ones are mechanically hard and not water soluble- the Perovskites and other metal oxides with related structure belong to this group. The other class are mechanically soft and water soluble. The harder ones have a larger polarisation usually due to created dipoles and the soft ones have a smaller polarisation due to an ordering of dipoles.

1.2 ANTIFERROELECTRICS

The concept of antiferroelectricity arose when it was suspected that certain materials showing a high dielectric constant peak and obeying Curie-Weiss law above an inversion could be nonpolar rather than ferroelectric below the transition. Kittel(4) developed the concept of antiferroelectricity before it had been recognised experimentally and made a number of predictions most of which have been borne out by later experimentation. He postulated an antiferroelectric to be a material whose subcells showed a polar arrangement but in which adjacent subcells were oppositely polarised giving a net zero polarisation and a centre of symmetry. Hence the antiferroelectric phase will not be piezoelectric.

Jona and Shirane define antiferroelectric as "an antipolar crystal whose free energy is comparable to polar crystal". The consequence of this definition can be seen as follows. The repeat unit cell in the antiferroelectric range is a multiple of the unit cell found above the transition. Since the antiferroelectric phase is nonpolar, it has no spontaneous polarisation referred to the multiple cell- hence it can show no hysteresis loop similar to the ferroelectric phase, under reasonable fields. However, in some antiferroelectrics double loops are observed under large fields of the order of 30 KV/cm. This is because the material becomes ferroelectric when acted upon by a sufficiently large field. This implies that there exists a ferroelectric structure with free energy only slightly greater, in the absence of a field, than that of the stable antiferroelectric structure, e.g., PbZrO_3 (Shirane et al(5)).

1.3 CRITERIA OF FERROELECTRICITY

Sometimes it is hard to decide whether a crystalline substance is or is not ferroelectric. Each unit cell of a ferroelectric crystal carries a reversible electric dipole moment, spontaneously oriented parallel to the dipoles of the neighbouring cells. The dipole moment can be the resultant of the charges of a simple array of ions as in a perovskite cell or a very complex arrangement in a multiple cell. Under attainable fields, the dipole moment must be reversible in direction by 180° and sometimes by other discrete smaller angles that correspond to various axes of the cell. By definition it is this reversibility of dipoles by a field that constitutes ferroelectricity. Because of the random orientation of crystallites, ferroelectricity is harder to

demonstrate in a ceramic than in a single crystal. In instances where a ceramic doesn't show dipole reversibility but a single crystal does so, it seems fair to consider the ceramic as ferroelectric. Most of the ferroelectrics have a Curie point above which they are nonpolar. However, of all the attributes only the demonstrated reversibility of an electric moment that arises from a polar unit cell is the true effect.

1.3.1 Dielectric Hysteresis

The commonly accepted criterion of ferroelectricity is a hysteresis loop on a D-E display. This is usually done with a modified Sawyer and Tower(6) circuit as shown in Fig. 1. The method consists of applying an alternating voltage and relating the stored charge to the instantaneous voltage. A large integrating capacitor C_s is placed in series with the sample. The voltage across it measures the charge stored in the test capacitor, and is conventionally displayed as the vertical deflection of an oscilloscope. The applied high voltage is displayed as the horizontal deflection. The various parameters in the hysteresis loop are measured in the usual way. The hysteresis results from the energy needed to reverse the metastable dipoles during each excursion of the field. The area of the loop is the energy dissipated as heat within the sample. Nonlinearity of the resistance of the sample and its conduction can be taken care of by modifying the circuit suitably.

1.3.2 Dielectric Constant

The one other possible evidence of ferroelectricity could be the high dielectric constant associated with the transition from polar to nonpolar phase.

The existence of a dielectric anomaly is not of itself a proof of

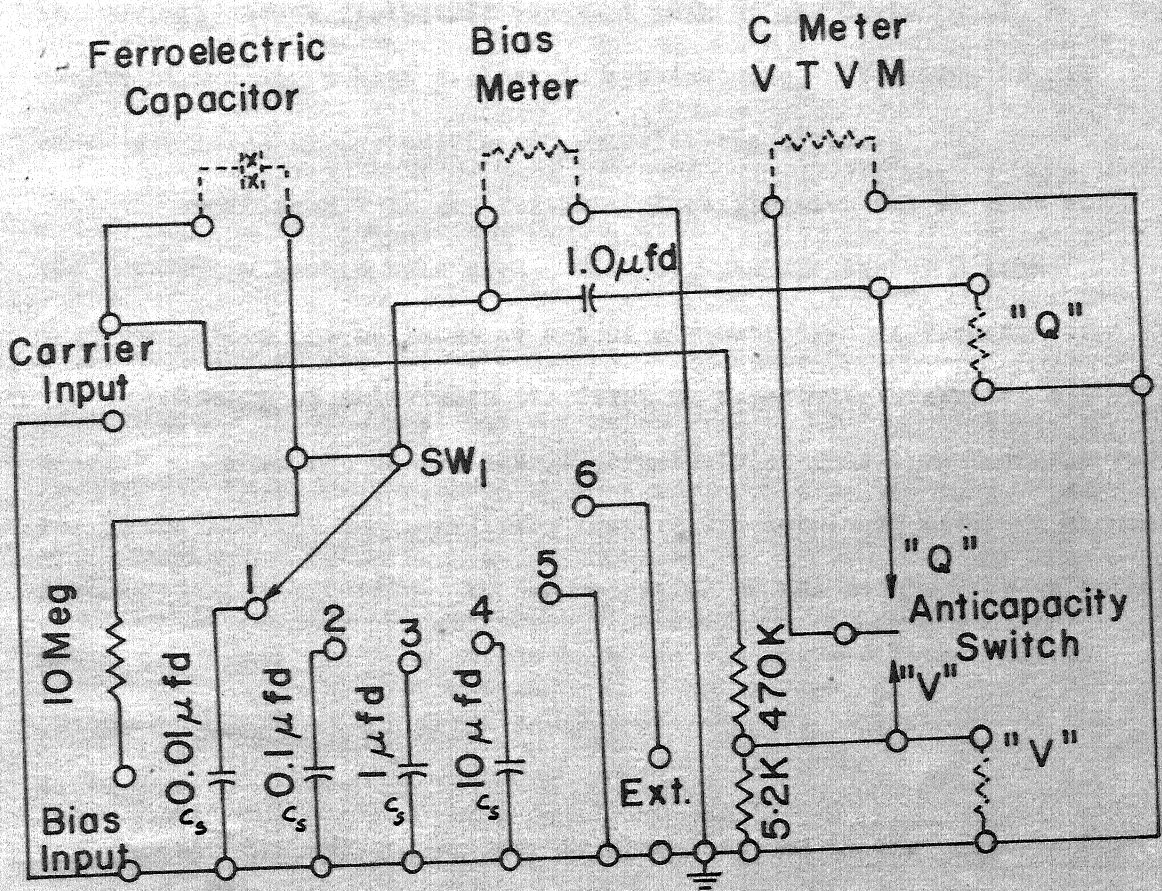


FIG.1. Wiring diagram of the ferroelectric analyzer .

ferroelectric transition since antiferroelectric transitions have associated with them such anomalies. In addition, large classes of materials undergoing various structural and hindered rotation transitions will also exhibit discontinuities or breaks in the plots of dielectric constant versus temperature, which will not have ferroelectricity associated with them.

A true ferroelectric has a true dielectric hysteresis. It also has a polar structure and has a finite spontaneous polarisation. It generally has a dielectric constant peak at the Curie point, a domain structure, a high dielectric constant etc. If poled, it can show reversible piezoelectric and pyroelectric effects.

Thus for a true and definite classification all or most of the properties should hold good. However, the display of a true hysteresis loop can be taken as a true demonstration of ferroelectricity.

Kanzig et al(7) were the first to report the effect of a biasing field on the ferroelectric-paraelectric transition temperature. For ferroelectrics the transition temperature increases with the biasing fields. This was followed by demonstration of the double loop in BaTiO_3 above the transition temperature by Cross(8). Here a ferroelectric phase is induced on the paraelectric phase by the application of the field.

Antiferroelectrics are nonpolar referred to the multiple cell and hence do not show dielectric hysteresis. Shirane et al(5) first observed double hysteresis in lead zirconate over a temperature range of a few centigrade degrees below the inversion temperature. Here a ferroelectric phase is induced on a nonpolar phase because the free energy difference between the two phases are small.

1.3.3 Other Considerations

A ferroelectric transition is always associated with it a volume contraction and an antiferroelectric transition with a volume expansion. In antiferroelectrics unlike in ferroelectrics, the application of the biasing field reduced the inversion temperature.

To demonstrate distinctly that a particular material is ferroelectric or antiferroelectric, all the physical properties mentioned above will have to be studied. Thus the distinction between the two is not clear cut; both have a dielectric anomaly and both can show double loops under suitable conditions.

One more test would be the one done by Shirane et al(5). The specimen was first cooled through the transition in an electric field and its faces were shorted through a galvanometer. On subsequent heating the discharge current was observed at the transition. For a ferroelectric there would be a discharge current because of the sudden destruction of spontaneous polarisation and zero current in an antiferroelectric as it is nonpolar.

1.4 THEORY OF FERRO- ANTIFERRO- ELECTRICITY

From the electrostatic relations in a linear isotropic dielectric medium, the dielectric constant is given by

$$\epsilon = D/E = \frac{E + 4\pi P}{E} \quad (1.1)$$

where ϵ is the dielectric constant, D is the dielectric displacement, E is the electric field, and P is the polarisation of the medium.

This analysis neglects the field at each atom owing to the fact that the other atoms are polarised. Lorentz treated this problem by

imagining a fictitious cavity cut around the position of the atom at which the value of the electric field is desired and then calculating separately the local field produced at the centre of the cavity in a uniformly polarised medium and the field due to the polarised matter contained in the cavity. He arrived at a general expression for the effective field (E_{eff}) as

$$E_{eff} = E_{appl} + \frac{1}{3} P \quad (1.2)$$

(Ref. C. Kittel)

where $\frac{1}{3}$ is the Lorentz factor.

For not too dense a medium, such as a gas it can be shown (Ref. C. Kittel) that

$$P = \frac{N \alpha}{(1 - \frac{1}{3} N \alpha)} \quad (1.3)$$

and

$$\frac{\epsilon - 1}{4 \pi} = \frac{N \alpha}{(1 - \frac{4 \pi}{3} N \alpha)} \quad (1.4)$$

where α is the polarizability of the ions constituting the medium.

Thus if $\frac{4 \pi}{3} N \alpha$ tends to 1 the medium is polarised in the absence of a field. More specifically if by some mechanism the quantity $\frac{4 \pi}{3} N \alpha$ can be shown to vary with temperature such that

$$\frac{4 \pi}{3} N \alpha = 1 - \beta (T - T_c)$$

then

$$\frac{\epsilon - 1}{4\pi} = \frac{1}{(4\pi/3)} \times \frac{1}{\beta(T-T_c)} \quad (1.5)$$

This when applied to the case of water, with the dipole moment of water molecules equal to p would result in a relation

$$\epsilon = 1 + \frac{4\pi N p^2}{3k(T-T_c)} \quad (1.6)$$

i.e., water would become ferroelectric at $T_c = 1000^\circ\text{K}$ and in practice this doesn't occur.

Onsager(9) provided a reason why the "Lorentz Catastrophe" predicted in many polar liquids does not occur. This is due to the fact that random thermal fluctuations of molecules do not take the same form for systems in which there occurs strong coupling as in widely separated dipoles. That is, correlation effects among neighbouring dipoles cannot be neglected in treating thermal fluctuations. When these are taken into account, no polarisation catastrophe is predicted.

1.4.1 Phenomenological Theory

In the phenomenological approach one expands the Helmholtz free energy as a power series in the polarisation and examines the various experimentally determined quantities related to ferroelectric behaviour of a solid. For a crystal which is not piezoelectric in its paraelectric state, the Helmholtz free energy is expressed as

$$F(P,T) = AP^2 + BP^4 + CP^6 + \dots + F_0(T) \quad (1.7)$$

where $F(P,T)$ is the free energy expressed as a function of the electric polarisation and temperature. A , B and C are coefficients expressing

the dependence of the free energy on the polarisation. $F_0(T)$ is the normal free energy associated with the interactions other than those that are polarisation dependent. The assumptions involved in the above equation are (a) the crystal is free and (b) P is the component of the polarisation vector along the ferroelectric axis. Coefficients A , B and C may be temperature dependent. For the case of a crystal which is nonpolar above the Curie temperature, the power series must contain only even terms, since the free energy should not depend upon whether the crystal is polarised up or down.

The differential form of the Helmholtz free energy is

$$dF = -Xdx + EdP - SdT \quad (1.8)$$

where X is the generalised force, x is the generalised displacement (strain in this case), S is the entropy and T is the temperature.

From eqns. (1.7) and (1.8) it follows that

$$\frac{\partial F}{\partial P} = E = 2AP + 4BP^3 + 6CP^5 + \dots \quad (1.9)$$

$$\frac{\partial^2 F}{\partial P^2} = \frac{\partial E}{\partial P} = \frac{4\pi}{\epsilon - 1} = 2A + 12BP^2 + 30CP^4 \quad (1.10)$$

$$\frac{\partial F}{\partial T} = -S \quad (1.11)$$

Thermodynamically, the equilibrium state corresponds to the minimum of free energy. The eqn. (1.9) has a trivial solution of $E = 0$ for $P = 0$. If this point $P = 0$ represents a minimum in F , $(F(P,T) - F_0(T))$, then this state (nonferroelectric) is the equilibrium state.

On the other hand if

$$2AP + 4BP^3 + 6CP^5 = 0 \quad (1.12)$$

has a nontrivial real solution for which F is minimum, then the equilibrium state will be determined by which value of P (nontrivial solution of eqn. (1.12)) leads to a lower value of F .

By the above phenomenological approach it has been found that the behaviour of a number of ferroelectrics can be predicted if it is assumed that A has a temperature dependence of the form

$$A = a(T - T_c) \quad (1.13)$$

where a is a constant. Experimentally two different cases have been found. One for which B and C are positive and the other with B negative and C positive. For the case where B is positive it is found, with $T > T_c$ (i.e., A is positive), there is only one minimum in F , namely, at $P = 0$. That is, the crystal remains paraelectric. For $T < T_c$ two minima appear at $\pm P_s$ with P_s depending on T (P_s is the spontaneous polarisation). That is, the crystal is ferroelectric.

The value of the dielectric constant in either case is from eqns. (1.10) and (1.13)

$$\frac{4\bar{\epsilon}}{\epsilon - 1} \simeq \frac{4\bar{\epsilon}}{\epsilon} = 2a(T - T_c) + 12BP^2 + 30P^4C \quad (1.14)$$

for $T > T_c$, $P = 0$ and then

$$\epsilon = \frac{(2\bar{\epsilon}/a)}{(T - T_c)} \quad (1.15)$$

Thus ϵ exhibits Curie-Weiss behaviour.

For $T < T_c$ eqn. (1.12) has a solution

$$P^2 = -\frac{A}{2B} = -\frac{a(T - T_c)}{2B} \quad (1.16)$$

if P^4 is neglected in eqn. (1.12). That is, this solution is good

only for small value of P , i.e., near T_c . Then from eqn. (1.14) and (1.16) the dielectric constant in the ferroelectric phase is given by

$$\frac{4\overline{\epsilon}}{\epsilon} = 2A + 12B\left(\frac{-A}{2B}\right) = -4A = -4a(T-T_c) \quad (1.17)$$

Thus ϵ^{-1} variation with temperature is linear above and below T_c with $\epsilon^{-1} = 0$ at T_c and the two slopes are opposite in nature. The slope below T_c is negative and is twice that of the one above T_c . This has been found to be more or less correct in the case of triglycine sulfate, ref: (Triebwasser(10)).

BaTiO_3 and KNbO_3 are the cases for which B is negative. The transition between phases occurs when the temperature for which the nonzero solution of $\frac{\partial F}{\partial P} = 0$ has the same free energy as that for $P = 0$. At this temperature P changes discontinuously from $P = 0$ to $P = P_s$. From eqn. (1.11) it is seen that there is an entropy change associated with a change in polarisation. If it is assumed that B and C are temperature independent then from eqn. (1.11)

$$\Delta S = S_{\text{ferro}} - S_{\text{para}} = aP_s^2$$

This entropy change will be associated with it a latent heat, $T \Delta S$, i.e.,

$$L = T \cdot \Delta S = T_c aP_s^2.$$

Materials with B negative (e.g., BaTiO_3) suffer a discontinuous change in P at T_c and latent heats have been measured in them, indicating thereby that the transition is of the first order. With B positive, there is no discontinuous change in P and no change in heat content. Hence these materials undergo a second order transition, exhibiting an anomaly in heat capacity but no latent heat of transition.

Thus the phenomenological approach seems to indicate that the interactions with which ferroelectricity is associated can be regarded as small perturbations rather than major contributors to the lattice energy.

1.4.2 Devonshire-Slater Theory of BaTiO₃

Theories exploring the ferroelectric interactions on a microscopic scale have been applied with reasonable success to KH_2PO_4 and BaTiO_3 . The Lorentz field type of calculations have been performed in detail with the latter. Devonshire(11) attempted to justify his assumed free energy function by an analysis of ionic polarizability in the BaTiO_3 lattice. In this treatment each cell of the array of cubic cells has in it a charged particle (e.g., Ti^{4+} ion) which is in equilibrium under various forces originating from coulomb interactions and short range quantum mechanical forces. In the presence of a local field, such a charged particle will be displaced from its equilibrium position, resulting in an effective dipole polarisation of each cell. This constitutes a polarisation of the lattice. The important distinguishing characteristic of this treatment is the fact that the lattice cells have no intrinsic polarisation but only an induced polarisation. The actual form of eqn. (1.14) can be derived by assuming a reasonable dependence of the force field on small displacements from the equilibrium position.

Slater(12) treated the problem in a similar manner but took the detailed structure into account more exactly by calculating the Lorentz fields for each of the four different interpenetrating cubic lattices. Thus in BaTiO_3 if Z direction is considered as the polar direction, (i.e., the induced dipoles are to be lined up along Z axis) then it is found that the Ti-O interaction is such that an array of dipoles on either

set of sites causes a strongly enhanced field on the other. To be more explicit, Slater showed by such a treatment that the field generated at the Ti site by a polarisation, P_o , associated with the array of polarised O_z ions is larger than $\frac{4\pi}{3} P_o$ by a factor of 9. The field at the O_z ions generated by an array of dipoles at the Ti position having polarisation P_{Ti} is also 9 times as large as the Lorentz value. It is this extraordinarily strong interaction which makes the perovskite structure favourable for ferroelectric interactions. In fact, all ABO_3 materials exhibit high dielectric constant whether or not they are ferroelectric.

From the known electronic polarizabilities and published structural data it is possible to calculate the total polarisation of the lattice, leaving only one adjustable parameter - namely, the ionic polarizability of one of the species of atom. A number of interesting results follow from the above model. The magnitude of local fields that are found are quite revealing in demonstrating what is going on. In the paraelectric state the local field is much larger than the applied field by a factor of approximately the dielectric constant which is of the order of 10^4 . Thus large polarising fields occur owing to the favourable arrangement of atoms in the lattice. The ratio of fields at various sites is 1.38:0.031:1.05:0.165 at the Ti, Ba, O_z and O_x or O_y sites respectively. Hence the fields along Ti - O_z line are about ten times as great as at other sites in the lattice. The same calculation also reveals that the Ti contributes 15%, the O_z 57%, O_x and O_y 13% each, and the Ba 1% to the total polarisation. Thus here the effect of high polarizability of oxygen ion is seen.

The next step is the calculation of the only adjustable parameter - namely, the ionic polarizability from microscopic short range forces. In spite of the meagre knowledge of these forces, quite reasonable qualitative agreement

with eqn. (1.7) has been achieved with regard to the order of magnitude of the various coefficients such as A, B etc. and the variation with temperature. No better agreement can be achieved with these theories because of the fundamental assumption of treating the ions as point charges.

Megaw(13) studied the ABO_3 compounds from a structural standpoint. She presents a rather qualitative model of ferroelectricity and antiferroelectricity in the perovskites which relates volume and allowed bond angles in the TiO_6 - like Octahedra. This kind of treatment, which depends heavily on bond arrangement, is weakened considerably by the success of the phenomenological approaches.

Jaynes(14) examined the Lorentz field type of treatment given by Devonshire and Slater and pointed that the basic assumptions contained in this type of analysis may be crude. Fundamentally the assumption of the existence of point charges and point dipoles represents a poor approximation when it is considered that the actual size of the ions involved is of the order of half the cell size, and the Lorentz field does vary with the position in the unit cell. Further it has been shown that the ionic polarizability of the constituent ions in particular O^{2-} , is a function of the lattice in which the ions are contained (J.R. Tessman et al(15)).

Jaynes considers that the high polarizability comes about by a perturbation of the electronic states of the TiO_6 octahedra in $BaTiO_3$ by the local electric field. Such an analysis can be more revealing than the point dipole model in treating the problem of short range forces. Unfortunately this model suffers from the problem of trying to assign an internal electric field to a structure which essentially occupies the entire cell. Further there is no reasonable way in Jayne's work to take

into account the ionic displacements that have since been demonstrated conclusively by neutron diffraction studies. The electronic theory, however, presents an interesting exercise which will become more useful when more is learnt about electronic structure of ionic or partially ionic crystals.

1.4.3 Lattice Dynamical Theory

The most promising method of dealing with the problem of ferroelectricity at the present stage, seems to be that of treating it as a problem in lattice dynamics. This approach is based on the probable existence of a low frequency optical vibration just above T_c of those ferroelectrics which show a large anomaly of the dielectric constant.

For the case of zero damping the dispersion formula for the dielectric constant is

$$\epsilon(\omega) = \epsilon_{\infty} + \sum_i \frac{b_i^2}{\omega_i^2 - \omega^2} \quad (1.18)$$

(Born and Huang(16)),

where ϵ_{∞} is the optical dielectric constant, ω_i is a measure of the strength of the restoring force related to the i^{th} optical mode and b_i is the strength of the coupling of this mode to the applied field E .

The static dielectric constant is given as

$$\epsilon_0 = \epsilon_{\infty} + \sum_i \frac{b_i^2}{\omega_i^2} \quad (1.19)$$

This is the one which becomes very large at T_c since ϵ_{∞} is only slightly temperature dependent. Thus for an anomaly in ϵ_0 , the second term in eqn. (1.19) should become very large. Assuming that the coupling constants b_i remain essentially finite at all temperatures of interest,

one would conclude that the restoring force of at least one of the vibrational modes considered here becomes very small or zero at T_c . It is thus logical to postulate that this particular restoring force is proportional to $(T - T_c)$ so that eqn. (1.19) assumes the form of Curie-Weiss law. This particular mode can be termed as the ferroelectric mode.

Dick and Overhauser(17) proposed a model for the dielectric behaviour of alkali halides on the recognition that the outer electrons of an ion, being less tightly bound, are more profoundly affected by the application of an electric field than the inner electrons. Accordingly the ions with rare gas configurations are regarded as consisting of an outer spherical shell of n electrons and a core constituted by the nucleus and the remaining electrons. In an electric field, shell retains its spherical charge distribution but moves bodily with respect to the core. The polarizability is made finite by a harmonic restoring force which acts between the core and the shell. The two unknown parameters, n and the spring constant of the restoring force are chosen by considering the polarizability and ultraviolet dispersion of a gas of such model ions. Using this model, they introduced two polarisation mechanisms which are neglected in the simple dielectric theory, namely, the short range interaction polarisation and the exchange charge polarisation. The short range interaction arises when pairs of positive and negative ions are moved toward each other because the shells of the ions repel one another and tend to become displaced with respect to the ion cores. This is equivalent to the polarisation of the ions, which may have different values for negative and positive ions depending on the spring constants and the shell charges ne . The exchange polarisation arises from the overlap of the

ions and the resulting exchange charge. This alteration of the exchange charge distribution is responsible for the repulsive force between nearest neighbours and gives rise to a net dipole moment per unit volume. This shell model has been found to give a satisfactory explanation of the dielectric properties of alkali halides and of the lattice dynamics of sodium chloride.

It was shown by Born and Huang(16) that the condition that a crystal should be stable for all small deformations is that all the normal modes should have real frequencies. The limit of stability against a particular mode of vibration is approached as the corresponding frequency tends to zero.

On the basis of this and the model of Dick and Overhauser, Cochran(18), based his theory of ferroelectricity in crystals. For a diatomic cubic crystal, he arrives at expressions for the frequencies of the transverse optic (T.O)N and longitudinal optical (L.O) modes of wave vector zero as

$$\bar{M} \omega_T^2 = R'_0 - \frac{4\pi}{9V} (\epsilon_\infty + 2) (Z'e)^2 \quad (1.20)$$

$$\bar{M} \omega_L^2 = R'_0 + \frac{8\pi}{9V\epsilon_\infty} (\epsilon_\infty + 2) (Z'e)^2 \quad (1.21)$$

where \bar{M} is the reduced mass, V the volume of the unit cell, $Z'e$ the effective ionic charge, and R'_0 the short range restoring force. The second term in eqns. (1.20) and (1.21) arises out of coulomb interaction. The theory also shows that ω_T may approach zero without the crystal becoming unstable against other vibration modes. The quantities on the right of the equation (1.20) may be temperature dependent as the lattice vibrations are in practice not completely harmonic so that near $T = T_c$ one may write

$$\frac{\bar{M} \omega_T^2}{R'_0} = 1 - \frac{4\pi}{9VR'_0} (\epsilon_\infty + 2) (Z'e)^2$$

where γ is the temperature coefficient. Using the relation of Lydanne et al(19) that

$$\frac{\omega_L^2}{\omega_T^2} = \epsilon_0 / \epsilon_\infty$$

the Curie-Weiss law is obtained as

$$\epsilon_0 - \epsilon_\infty = \frac{4\pi}{9VR_0'} (\epsilon_\infty + 2)^2 (Z'e)^2 \frac{1}{T - T_c} \quad (1.23)$$

with the Curie constant $C \sim \frac{\epsilon_\infty + 2}{\gamma}$. Thus from eqns. (1.22) and (1.23) as T tends to T_c it is clear that ω_T^2 tends to zero and that ϵ_0 tends to ∞ .

The $\frac{4\pi}{3}$ catastrophe can be seen as follows. The ionic and electronic polarizabilities are

$$\alpha_{ion} = \frac{(Z'e)^2}{R_0'} \quad \text{and} \quad \alpha_{ele} = \frac{3V}{4} \left(\frac{\epsilon_\infty - 1}{\epsilon_\infty + 2} \right).$$

$$\text{For } \omega_T^2 = 0, \quad \frac{4\pi}{3} (\alpha_{ion} + \alpha_{ele}) = 1 \quad (1.24)$$

These above considerations apply to a diatomic cubic crystal in which each atom has surroundings of tetrahedral symmetry. A crystal having this symmetry but with n -atoms in the primitive unit cell, has in general for zero wave vector ($q = 0$), n transverse modes (each is degenerate) and n longitudinal modes. For such a case Cochran has shown that the relation corresponding to Lydanne et al is given as

$$\frac{\epsilon_s}{\epsilon_e} = \frac{n}{\sum_{j=2}^n} \frac{(\omega_j^2)_L}{(\omega_j^2)_T} \quad (1.25)$$

ϵ_s and ϵ_e are the static and optical dielectric constants. $(\omega_j)_L$ and $(\omega_j)_T$ are the frequencies of the longitudinal and transverse optical modes for $q = 0$. The dependence of ϵ_s on temperature for ferroelectric

materials in the ferroelectric region is given by Curie-Weiss law as

$$\epsilon_s = \frac{4\pi C}{(T - T_c)} \quad C \text{ is the Curie-Weiss constant.}$$

To explain the Curie-Weiss law Cochran has again shown that it is sufficient if one anomalous frequency ω_{an} of the homogenous transverse optical mode depends on the temperature as

$$\omega_{an}^2 = \gamma (T - T_c) \quad (1.26)$$

and other optical frequencies are temperature independent. Similar to the diatomic case it is the coulomb interactions, which act in the anomalous transverse optical mode against short range forces and thus decrease ω_{an} , are responsible for dependence as in eqn. (1.26).

Measurement of the inelastic scattering of slow neutrons (1.20) and optical measurements in the far infrared region carried out in SrTiO_3 (20) have confirmed the assumed dependence as in eqn. (1.26).

For the course of the anomalous branch for the nonzero \bar{q} , the following has been deduced by Anderson(21). He has shown that the Lorentz factors determining the local electric field decrease with increasing \bar{q} . Hence it can be expected that coulomb interactions will play substantial role only in the region of wave vectors close to zero. The correctness of this conception is again borne out by neutron measurements in SrTiO_3 (22).

Cochran also suggested that a transition to an antiferroelectric state can also be considered as the result of instability of a lattice vibrational mode. The ionic displacements associated with this mode would yield a nonpolar structure. The antiferroelectrics like PbZrO_3 obey Curie-Weiss law above T_c and have Curie constants of the same order of magnitude as that of their isomorphous ferroelectric substances.

This suggests that these antiferroelectric materials have associated with them an infrared active frequency whose temperature dependence can be given as in eqn. (1.22).

Cochran(18) showed that the antiferroelectric transition is connected with the instability of the crystal lattice with respect to the optical transverse phonons with wave vectors lying at the edge of the Brillouin zone. In other words in the neighbourhood of the antiferroelectric transition the energy of the phonons belonging to the end of the optical transverse branch will be anomalously low and strongly temperature dependent. Thus the energy of the phonons belonging to the beginning ($\bar{q} = 0$) of the optical transverse branch will also be small and temperature dependent.

The temperature dependence of this optical branch in crystals of the perovskite type was studied in detail by Silverman(23). His expression for the temperature dependent frequency of transverse optical modes from the linearised chain model is

$$\omega_T^2(q) = \gamma (T - (T_c + \Delta T(q))) \quad (1.27)$$

For an antiferroelectric $\Delta T(q)$ has its maximum value for \bar{q} belonging to the edge of the Brillouin zone; with decreasing \bar{q} it decreases and is equal to zero for $\bar{q} = 0$. Thus in antiferroelectrics in contrast to the ferroelectrics the whole of the transverse optical branch is temperature dependent.

CHAPTER - II

MOSSBAUER EFFECT

The Mossbauer effect is based on a resonance effect- namely, ' γ ' ray resonance absorption and emission. Resonance is a familiar phenomenon in all fields of physics and technology involved in vibrations and waves, such as sound waves, surface waves and electromagnetic waves. Unlike in long wave electromagnetic radiations certain basic conditions are to be satisfied for the short wave ' γ ' radiation resonance. The source used for observation of Mossbauer effect is a group of radioactive nuclei which in the last stage of their disintegration, decay from the excited state 'A' to the ground state 'G' of a stable nucleus emitting a ' γ ' ray in the process. When this radiation is incident on a substance containing the identical nucleus one would expect at first sight that the radiation would be absorbed by a resonance effect, in which the stable nucleus goes to the excited state. This is not observed for a closer consideration would show that this is quite understandable having regard to changes in energy and momentum that occur in a ' γ ' quantum that is emitted by a nucleus.

For a free atomic or nuclear system of mass 'M' with two levels separated by an energy ' E_0 ', the nucleus in the excited state will have an energy ' E_0 ' and zero momentum.

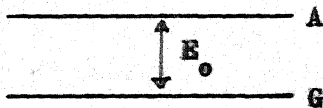


Fig. 2.1

If the system decays from A to G (Fig. 2.1) by emission of a photon of

energy E_γ , momentum conservation demands that the momentum p of the photon = $\frac{h f}{c}$ where f is the frequency of the photon and c is the velocity of light, and the momentum of the recoiling nucleus must be equal and opposite. Hence recoiling system receives an energy

$$R = \frac{p^2}{2M} = \frac{E_o^2}{2Mc^2} \sim \frac{E_\gamma^2}{2Mc^2} \quad (2.1)$$

Energy conservation requires

$$E_o = E_\gamma + R$$

since

$$R \ll E_\gamma \quad R \sim \frac{E_o^2}{2Mc^2} \quad (2.2)$$

Also if τ is the mean life of the excited state A against decay, then from uncertainty principle it follows that the energy of the excited field cannot be measured sharply but only within an uncertainty given by $\tau \Gamma = \hbar$ where Γ is the width of the energy band of the excited state. Actually the excited state cannot be characterised by one well defined energy E_o but only by an energy distribution centred around E_o . Photons emitted in the transition 'A' to 'G' thus would show a distribution in energy E_γ centred around $E_o - R$ and displaying a natural line width. The line width Γ corresponding to a mean life $\tau = 10^{-8}$ sec. is about 10^{-7} ev.

Thus when a photon of energy E_γ strikes a target of mass M which is initially at rest the entire momentum p is transferred to the target. The target thus recoils and the recoil energy is again given

by

$$R = \frac{p^2}{2M} = \frac{E_\gamma^2}{2Mc^2} \quad (2.3)$$

This energy must be supplied by the ' γ ' ray. Thus only an energy $E_\gamma - R$ is available for the excitation of the internal degrees of freedom. Hence to excite a level of energy E_0 , the incoming ' γ ' ray energy must be centred around $E_0 + R$. Resonance fluorescence can occur only if some of the incoming photons possess enough energy to reach the state A and at the same time provide the necessary recoil energy R to the receiving system. Thus only the overlapping part of the two spectra centred around $E_0 - R$ and $E_0 + R$ are responsible for fluorescence. That is, the condition for overlap is $2R \leq \Gamma$. Thus this condition is fully met in optical transitions and hence the resonance effect is observed.

If the thermal motion of the source and the absorber are also taken into consideration, the additional thermal broadening, namely, the Doppler broadening, would be

$$D \simeq 2 (\bar{\epsilon} R)^{\frac{1}{2}} \quad (2.4)$$

where $\bar{\epsilon}$ is the average kinetic energy of the emitters. Thus Γ is not the only dominant part in resonance fluorescence.

For optical radiations $R < D$, emission and absorption lines overlap and resonance conditions are obtained, whereas for nuclear transitions R is either comparable to or greater than D and thus resonance is not always possible.

In nuclear experiments though the conditions for resonance are violated, they can be restored by several means, e.g., heating up the

source and absorber to increase the average kinetic energy and hence the overlap of the emission and absorption spectra or by rotating the source at a high speed in a rotor with the source at the tip of the rotor so that the ' γ ' rays emitted tangentially gain additional energy to compensate recoil losses (Moon(24)). However, R.L. Mössbauer's discovery is unique in the sense that none of the above considerations are necessary.

Mössbauer was able to prove a "no phonon" absorption process, i.e., the process in which the resonant nucleus embedded in a lattice absorbs a ' γ ' ray photon and no energy is exchanged with the host crystal (i.e., $R=0$). That is, the vibration energy of the host crystal is the same after the absorption takes place, as it was before it.

However, the nuclear fluorescence in practice is more complicated because the nucleus is not perfectly rigidly bound to the crystal lattice, also the bond is not so weak that the nucleus is dislodged from its position due to recoil- the ' γ ' rays involved are too soft for that. The recoil momentum is, therefore, absorbed by the whole lattice. It is, however, possible that the recoil energy is lost by the gamma radiations because vibrations are generated in the not completely rigid crystal lattice, which are ultimately dissipated as heat.

Thus the theoretical treatments involve the coupling of two quantized systems; one, the nucleus which effects a transition between two energy levels while emitting the gamma ray and, two, the lattice vibrations which are excited during the emission through mechanical coupling.

2.1 CLASSICAL APPROACH

Regarding the nucleus as a radiation source of frequency f , since

the nucleus is always subjected to thermal vibrations, the emitted electromagnetic wave would show a Doppler shift. If f_0 is the ideal (no vibration) frequency, then

$$f(t) = f_0 (1 + V(t)/c) \quad (2.5)$$

The time dependence of the electromagnetic field associated with this radiation for harmonic motion of the nucleus can be given as (Frauenfelder)

$$A(t) = A_0 \sum_{-\infty}^{+\infty} J_n \left(\frac{2\pi X_0}{\lambda} \right) \exp(i(\omega_0 + 2\pi nF)t) \quad (2.6)$$

with the amplitude of vibration of the source, $X(t)$, being $X(t) = X_0 \sin 2\pi Ft$. In eqn. (2.6) λ is the Doppler unshifted wavelength of the ' γ ' radiation.

Eqn. (2.6) represents an electromagnetic wave which is a superimposition of partial waves of frequencies ω_0 , $\omega_0 \pm 2\pi F$ etc. Thus it is a spectrum of frequencies with the central line at f_0 and side bands at $f_0 \pm F$ etc. The amplitude of each wave is given by the Bessel function $J_n \left(\frac{2\pi X_0}{\lambda} \right)$. The unshifted line is the Mossbauer line whose intensity is

$$f = \left| A_{(n=0)} \right|^2 = J_0^2 \left(\frac{2\pi X_0}{\lambda} \right) \quad (2.7)$$

For the random movement of the source in a Debye solid

$$f = \prod_{m=1}^{3N} J_0^2 \left(\frac{2\pi X_m}{\lambda} \right) \quad (2.8)$$

Using the approximation

$$J_0(y) \simeq 1 - y^2/4 \quad \text{for small values of } y, \text{ we have}$$

$$\ln f \simeq -2 \sum_{m=1}^{3N} \frac{1}{4} \left(\frac{4\pi^2 X_m^2}{\lambda^2} \right) \quad (2.9)$$

$$\text{Since } \langle X^2 \rangle_{\text{ave}} = \frac{1}{2} \sum X_m^2$$

$$f = \exp \left(\frac{-4\pi^2 \langle X^2 \rangle}{\lambda^2} \right) \quad (2.10)$$

The physical interpretation here is that the continually emitted electromagnetic wave comes from a region of linear dimensions X^2 . If this linear dimension increases beyond $\left(\frac{\lambda}{4\pi}\right)$ pieces of the wave trains emitted from different points in this region interfere destructively and the fraction of photons emitted without energy loss decreases rapidly.

Since $\langle X^2 \rangle = 1/3 \langle r^2 \rangle$ and $\langle r^2 \rangle$ for a Debye solid is given as

$$\langle r^2 \rangle = \frac{9\hbar^2}{4mk_D} \left(1 + \frac{2\pi^2 T^2}{3\theta_D^2} \right) \quad (2.11)$$

(θ_D is the Debye temperature)

it follows that

$$f = \exp \left(-3/2 \times \frac{E_R}{k\theta_D} \left(1 + \frac{2\pi^2}{3} \frac{T^2}{\theta_D^2} \right) \right) \quad (2.12)$$

where $E_R = \frac{E_0^2}{2mc^2}$. This is called the Debye-Waller factor.

Instead of Debye's continuum model, if Born-Karman's lattice dynamical theory is evoked one would get the effect of the optical mode on 'f'. The result then would be

$$f = \exp \left(-\frac{E_R}{\hbar\omega_0} \coth \left(\frac{\hbar\omega_0}{2kT} \right) \right) \quad (2.13)$$

which means if two crystals have identical Debye temperature, with one being monoatomic and the other possesses a larger unit cell, 'f' factor will be greater with the more complicated structure.

Lipkin(25) has given a sum rule for the average energy transfer

to the lattice as

$$\sum_{n_f} (E_{n_f} - E_{n_i}) P(n_f, n_i) = \frac{(\hbar k)^2}{2M} \quad (2.14)$$

E_{n_f} and E_{n_i} are the energies of the lattice states n_f and n_i . $P(n_f, n_i)$ is the probability that the lattice will be in a state n_f from the initial state n_i after the transition. Thus the average energy transferred to the lattice is just the energy which the individual nucleus would if it recoiled freely. Mossbauer transition in which $E_{n_f} = E_{n_i}$ do not contribute to the sum rule. Thus for an appreciable probability that there be no energy transfer to the lattice, the sum rule requires an appreciable probability for an energy transfer which is greater than that which a freely recoiling nucleus would receive, i.e., in a lattice where the nucleus can transfer energy to high frequency lattice modes.

For calculating the probability $P(n_i, n_i)$ that the lattice remains in its initial state after the emission, it is assumed that the interatomic forces in the lattice are harmonic so that the vibrational modes can be represented by normal coordinates. Then

$$P(n_i, n_i) \simeq \exp \sum_s -((2n_s + 1) \left(\frac{\hbar^2 k^2}{2M\hbar\omega_s} \right) a_{LS}^2) \quad (2.15)$$

where a_{LS} is the normalisation constant. $\frac{\hbar^2 k^2}{2M\hbar\omega_s}$ is just the ratio of the free recoil energy to the energy of the s^{th} lattice vibration normal mode. At 0°K $n_s = 0$. The exponent in eqn. (2.15) then, is just the ratio of the free recoil energy to some average lattice vibration energy $\hbar\omega_{av}$ given as

$$(\hbar\omega_{av})^{-1} = \sum_s \frac{a_{LS}^2}{\hbar\omega_s}$$

For a Debye solid, set $a_{Ls} = a$ constant and take the density of lattice modes as proportional to ω_s^2 . Then

$$\begin{aligned} (\hbar \omega_{av})_{\text{Debye}} &= \frac{2}{3} \hbar \omega_{\text{max}} \\ &= \frac{2}{3} k \theta_D \end{aligned} \quad (2.16)$$

Then

$$P(n_i, n_i) = \exp \left(- \frac{3}{2} \frac{(\hbar k)^2}{2mk\theta_D} \right) \quad (2.17)$$

Thus all the above expressions (eqns. (2.15), (2.16), (2.17)) lead to the conclusion that the probability of gamma ray emission without energy transfer to or from the lattice increases with the average energy of the lattice mode which are coupled to the recoiling nucleus and the effect becomes appreciable when this average energy is of the same order of magnitude as the recoiling energy.

Summarising Lipkin's Sum rule, the characteristics of Mossbauer effect depend upon three parameters; namely, (1) the energy of the free recoil, (2) the characteristic temperature of the lattice, ((Debye temperature) and (3) the ambient temperature. To obtain the effect, the lattice temperature should be of the same order of magnitude as the recoil energy and the ambient temperature should be low. However, it is not always true that θ_D will be the main factor affecting f , for it is known that in some light elements it is their low mass rather than strong binding which gives them a high Debye temperature. The more complicated crystals should be chosen for strong binding of the source or absorber atoms rather than for high Debye temperature.

2.2 CONDITIONS FOR THE MOSSBAUER EFFECT

It is evident from the above critical considerations that for some of the gamma transitions in the nuclei of both source and absorber no lattice vibrations are involved. If the effect is to be observed, many such transitions could occur in both source and absorber. Hence the Mossbauer fraction is higher at low temperature and for softer gamma rays. Thus the nuclei transitions for which the Mossbauer effect has been observed, therefore, have $E_0 < 150 \text{ Kev}$ and for transitions above about 50 Kev cooling is necessary. Also the width of the excited state should not be too great. This limits the life time of the excited state to less than about 10^{-9} secs.

2.3 ISOMER SHIFT

By Mossbauer effect it is possible to compare the nuclear transitions in two materials with high precision. The nucleus is surrounded and penetrated by electronic charge with which it reacts electrostatically. The energy of interaction can be computed classically by considering a uniformly charged spherical nucleus imbedded in its s electron charge cloud. A change in s electron density, such as might arise from a change in valence, will result in an altered coulombic interaction which manifests itself as a shift in nuclear levels. The effect, however, depends on the difference in the nuclear radii of the ground and isomeric state.

For a point nucleus the electrostatic potential at a distance r from the nucleus is

$$V_{pt} = \frac{Ze}{r} \quad (2.17)$$

and for a finite nucleus of radius R

$$V = \frac{Ze}{R} \left(\frac{3}{2} - r^2/2R^2 \right) \quad \text{for } r \leq R \quad (2.18)$$

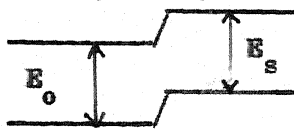
and

$$V = \frac{Ze}{r} \quad \text{for } r > R$$

The difference in energy can be given as (Werthiem)

$$\delta E = \frac{2\pi}{5} Ze^2 \left| \psi_s(0) \right|^2 R^2 \quad (2.19)$$

where $\left| \psi_s(0) \right|^2$ is the s electron density at the nucleus.



Thus for the source the energy difference between the ground and excited state can

For source

be given as

$$E_s = E_0 + \frac{2\pi}{5} Ze^2 \left| \psi_s(0) \right|^2 (R_{ex}^2 - R_{gd}^2) \quad (2.20)$$

Similarly for the absorber

$$E_a = E_0 + \frac{2\pi}{5} Ze^2 \left| \psi_a(0) \right|^2 (R_{ex}^2 - R_{gd}^2) \quad (2.21)$$

The Isomer shift (Werthiem)

$$I.S. = E_a - E_s = \frac{4\pi}{5} Ze^2 R^2 \left(\frac{\delta R}{R} \right) \left(\left| \psi_a(0) \right|^2 - \left| \psi_s(0) \right|^2 \right) \dots (2.22)$$

Eqn. (2.22) contains the electronic charge density at the nucleus which is basically an atomic or chemical parameter since it is affected by the valence state of the atom and the nuclear parameters R_{ex} and R_{gd} .

Thus in the absence of hyperfine splitting, the shift in the centre of the absorption line would throw light on the valence state of the probed ion provided the sign of δR is known. On the other hand,

on the assumption that the electronic charge density in an ionic salt is the same as in a free ion, the results of Hartee-Fock calculations can be used to find the chemical factor and hence a measure of would reveal the value and sign of δR . Systematics of Isomer Shifts of Fe^{57} as a function of 3d and 4s electron charge density has been developed by Walker et al(26). Similar systematics has been worked out for tin compounds by Kistner et al(27).

2.4 QUADRUPOLE COUPLING

When the spin I of an atomic nucleus is greater than $\frac{1}{2}$, its distribution of positive charge is nonspherical in shape. With respect to the spin axis, the ellipsoid charge can be either prolate or oblate. In case of prolate charge distribution, it can be imagined that the positive charge has migrated leading to an excess of positive charge at the north and south poles, balanced by a defect of positive charge at the equator. The opposite state of affairs occurs with the oblate distribution of charge. The nucleus then possesses an electric quadrupole moment Q which measures the deviation of the nuclear charge from spherical symmetry. In terms of nuclear dimensions

$$Q = \int r^2 \rho (3 \cos^2 \alpha - 1) d\tau \quad (2.23)$$

where ρ is the nuclear charge density, r is the distance from the centre of gravity of the charge to the volume element $d\tau$ and α is the angle between r and the spin axis.

In atoms and molecules nuclei are embedded in an electronic cloud. When the electrons and other charges outside a particular quadrupolar nucleus have a nonspherical charge distribution, there is

an interaction between the nuclear field and the external field. A nucleus possessing a quadrupole moment, situated in an inhomogeneous electric field, possesses a potential energy which depends upon the orientation of its quadrupole moment with respect to the external field. The possible orientations of the spin axis of a nucleus in a molecule relative to the axis of rotation of the molecule as a whole are quantized. When Q interacts with the electric field E , each of the allowed orientations may possess different potential energy. The quadrupole coupling energy of a single nucleus is proportional to eQq , where e is the proton charge and q is the field gradient. When the charge distribution of the electronic shells are spherically symmetric, $q = 0$. For an atom with one valence electron, the potential energy V due to this single electron at a distance r is

$$V = e/r$$

and

$$\frac{\partial^2 V}{\partial z^2} = e (3 \cos^2 \theta - 1) / r^3 \quad (2.24)$$

where θ is the angle between r and Z axis. When this is averaged over the orbital occupied by the electron, the contribution of the valence electron to q is

$$q = e \int \psi \left(\frac{3 \cos^2 \theta - 1}{r^3} \right) \psi^* d\tau \quad (2.25)$$

(Dailey et al(28))

where ψ is the wave function of the electron.

The field gradient in a general lattice is obtained by applying the gradient operator to the 3 components of the field, which itself is a

vector. Consequently the field gradient is a tensor of rank 3 and this referred to the principal axis can be reduced to the diagonal form so that it can be completely specified by $\frac{\partial^2 V}{\partial x^2}$, $\frac{\partial^2 V}{\partial y^2}$ and $\frac{\partial^2 V}{\partial z^2}$, all of which would be distinct for a triclinic lattice. Further, they obey the Laplace's equation, namely,

$$\sum V_{xx} = 0 \quad (2.26)$$

Defining an assymetry parameter γ as

$$\gamma = \frac{V_{xx} - V_{yy}}{V_{zz}}$$

where V 's are chosen such that

$$|V_{zz}| > |V_{xx}| \geq |V_{yy}|$$

so that $0 \leq \gamma \leq 1$, the interaction between Q and the field gradient is given as

$$H = Q \cdot \nabla E \quad (2.27)$$

whose eigenvalues would be

$$E_Q = \frac{eQq}{4I(2I-1)} (3m_I^2 - I(I+1)) (1 + \gamma^2/3)^{\frac{1}{2}} \quad (2.28)$$

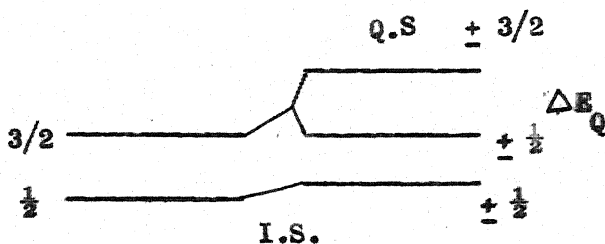
This expression contains only the second power of the magnetic quantum number, m_I , which means that the substates differing only by sign are still degenerate.

The two fundamental sources of effective field gradient (E.F.G.) are (1) the charges in the distant ions and (2) the electrons in the incomplete shell of the atom itself. Distant ions contribute to E.F.G.

provided the symmetry of the lattice is lower than cubic. If the crystal structure is known to high precision, and if an ionic charge can be assigned to the lattice sites, then the E.F.G. at the particular lattice site can be computed by the Lattice Sum method. This is greatly modified by the atom's own electrons whose wave functions are distorted by interaction with the external E.F.G. and as a result create their own E.F.G. This is the antishielding phenomenon and the antishielding factor for different ions has been evaluated by Stenmeier et al(29). Thus the effective E.F.G. is given by

$$q = q' (1 - \gamma_{\infty}) \quad (2.29)$$

where γ_{∞} is the Stenmeier's antishielding factor.



Referring to the above figure and eqns. (2.28) and (2.29) it can be seen that

$$\Delta E_Q = \frac{1}{2} e^2 (1 - \gamma_{\infty}) q Q (1 + \gamma^2/3)^{\frac{1}{2}} \quad (2.30)$$

Knowing the symmetry of the lattice, Q of the nucleus and the charge state of the ion it is possible in principle to calculate q .

For the typical case of Fe^{57} or Sn^{119} where the excited state gets split into $\pm 3/2$ and $\pm 1/2$ levels the relative intensities of the two Mossbauer lines would depend upon the orientation of the axis of symmetry to the propagation of gamma rays. In randomly oriented

crystallites, as in a powder sample, the orientations will have to be averaged over a sphere and the result would be that the two lines would be of equal intensity. However, it may be mentioned here that an asymmetry of the Lamb-Mossbauer factor is bound to introduce changes in the observed line intensities.

2.5 MOSSBAUER EFFECT AND FERROELECTRICITY

Dvořák et al(30) have studied the influence of the anomalous branch of the phonon spectrum of the ferroelectrics on the Mossbauer effect. The intensity of the Mossbauer line(30) is given as

$$W(E) = W_0(E) \exp \left(-2 \sum_{\alpha} Z_{\alpha} \right) \quad (2.31)$$

where α denotes the branch of the lattice vibration spectrum and Z_{α} a distribution function involving the mean number of phonons with energy $\hbar\omega$, and the distribution function $g(\omega)$ of the frequencies of the phonons in branch α and the recoil energy of the nucleus per branch α . Thus the intensity of the Mossbauer line is determined by the function $g(\omega)$, which consists of a normal part $g_n(\omega)$ and an anomalous part $g_a(\omega)$ associated with the ferroelectric transition. The normal part is temperature independent and the anomalous part has a temperature dependence of the form given in eqn. (1.26). They have shown that in the paraelectric phase the energy of these phonons (for $q = 0$) decreases with decreasing temperature and when the Curie temperature is reached the energy of these optical transverse phonons becomes zero. As a consequence, when the temperature of the crystal is lowered towards the ferroelectric transition temperature, the probability of the excitation of anomalous optical phonons increases.

This hence leads to a decrease in the probability of the Mossbauer effect.

The effect of similar anomalous vibrational spectrum in the antiferroelectric materials on the Mossbauer line intensity has been studied qualitatively by Dvořák(31). He has shown on the basis of Silverman's model(23) that in contrast to ferroelectrics of perovskite type where, only the long wave part of the transverse optical branch lies very low and is strongly temperature dependent, in antiferroelectrics the whole branch exhibits such properties. From this reason a greater relative decrease in the intensity of the Mossbauer line can be expected in the neighbourhood of antiferroelectric than of ferroelectric transitions.

Bhide et al(32) were among the first to report work on the Mossbauer effect in BaTiO_3 doped with iron, as a function of temperature. From the E.P.R. studies (Horning et al(33)) and also from the ionic radii and valence considerations it is known that Fe replaces Ti in BaTiO_3 and that the Curie temperature falls to zero as the mole percent of Fe exceeds 5% (Nishioka et al(34)).

On the surface of the as grown single crystals, about 100 Curie active aqueous solution of $\text{Co}^{57}\text{Cl}_2$ was evaporated and the active residue was thermally diffused for one hour in hydrogen atmosphere. By quenching these single crystals from 1100°C to room temperature, they were able to overcome the association of anion vacancies with the Fe^{3+} ion; for otherwise the presence of vacancies would give rise to their own quadrupole splitting due to the interaction between the net positive charge at the vacancy site and the Mossbauer ion, i.e., Fe^{3+} . The charge state of the Mossbauer ion was fixed from the observed Isomer Shift relative to an Fe^{57} enriched stainless steel absorber and using the systematics of Walker et al(26).

The room temperature quadrupole splitting was 0.46 mm/sec.

The two lines were of equal intensities as is required for a multidomain single crystal. On poling the crystals, by applying an electric field, the intensity ratio became 3:1. Thus proving that they arise out of quadrupolar splitting.

From eqn. (2.30), since $\gamma = 0$ for a tetragonal lattice, knowing the quadrupole moment of Fe^{57} , q was obtained from the experimentally observed ΔE . This agreed fairly well with the E.F.G. arrived at from the Lattice Sum Calculation on the assumption of an ionicity of about 60%.

Their measurements of 'f' as a function of temperature showed an anomaly around the Curie temperature as required by the Cochran's theory(18). Experimentally it was observed that the variation of ΔE with temperature was similar to the variation of P_s^2 (P_s is the spontaneous polarisation) with temperature, even though there is yet no theoretical correlation between the spontaneous polarisation and the field gradient at the assumed ferroelectrically active ion.

About the same time Bokov et al(35) of the Academy of Sciences (U.S.S.R.) reported similar measurements in BaTiO_3 doped with tin. They studied $\text{Ba}(\text{Ti}_{.8}\text{Sn}_{.2})\text{O}_3$ in polycrystalline form as absorber with Mg_2Sn source, kept at -193°C . The Curie point of this doped BaTiO_3 is -142°C . They also observed an anomaly in the variation of 'f' as a function of temperature around -142°C . Except the room temperature spectrum and the variation of the Mossbauer line intensity with temperature, they have not reported the values of other Mossbauer parameters and their variation with temperature. Similar anomaly in 'f' around the Curie point was reported

by Chekin et al(36) from the study of Mossbauer effect in $\text{Ba}(\text{Ti}_{.9}\text{Sn}_{.1})\text{O}_3$.

Sklyarevskii et al(37) investigated the variation of parameters of Mossbauer absorption spectrum of Fe^{57} nuclei in the ferroelectric $\text{Pb}(\text{Fe}_{.5}\text{Nb}_{.5})\text{O}_3$ as a function of temperature. To get a better absorption spectrum they used Fe^{57} enriched Fe_2O_3 in making the solid solution. The source was Co^{57} diffused in stainless steel. The room temperature I.S. was $0.52 \pm .02$ mm/sec corresponding to Fe^{3+} and ΔE was $0.37 \pm .02$ mm/sec. They observed an anomalous decrease in 'f' and a discontinuity in I.S. around T_c .

An interesting piece of work has been reported recently by Plotnikova et al(38) concerning the ferroelectric-ferromagnetic substance $\text{Pb}(\text{Fe}_{.5}\text{Ta}_{.5})\text{O}_3$ which has a Curie temperature $T_c = -40^\circ \text{C}$ and Neel temperature $T_N = -140^\circ \text{C}$. The measurements were carried out on a constant velocity mechanical set up with the source $\text{Co}^{57}(\text{Pb})$. Below the Neel temperature poorly resolved magnetic spectrum and between -140°C and -40°C a doublet was observed. In concurrence with Cochran's theory the Mossbauer line intensity underwent anomalous changes around T_c .

Identical studies were carried out with BaSnO_3 source and $\text{Ba}(\text{Ti}_{.9}\text{Sn}_{.1})\text{O}_3$, $\text{Pb}(\text{ZrSn})\text{O}_3$, etc. as absorbers. Surprisingly all the spectra of $\text{Ba}(\text{SnTi})\text{O}_3$ and of other tin containing systems had the form of a single Lorentzian with a width almost equal to that of natural tin. Spectra of these specimens showed no significant changes on passing through T_c .

Thus their report is contradictory to the earlier ones on the Mossbauer effect in ferroelectrics containing tin. In their systematic study of various titanate and zirconate solid solutions, they report that significant chemical shifts occur in solid solutions when B type ions

of an ABO_3 compound are replaced by ions of different electronegativity, whereas the replacement of A ions has virtually no effect on I.S. Apparently changes in B-O-B* bonds have appreciably greater effect on the electron density in the vicinity of B ions than changes in weaker A-B bonds, here B* is the impurity ion added.

CHAPTER - III

LEAD ZIRCONATE AND ITS MODIFIED COMPOUNDS

The existence of a marked dielectric anomaly in Lead Zirconate was first reported independently by Roberts(39) and Smolenskii(40) in 1950. Above the Curie temperature (230°C) the dielectric constant follows the Curie-Weiss law. Although the character of the dielectric anomaly is similar to that observed in BaTiO_3 , it exhibited a volume expansion on heating through the transition temperature. Subsequent careful studies of the dielectric and the structural properties of PbZrO_3 , by Sawaguchi et al(41) established that the phase occurring below 230°C is antiferroelectric.

The correct symmetry of the antiferroelectric phase was found to be orthorhombic, with cell parameters $a = 5.87 \text{ \AA}$, $b = 11.74 \text{ \AA}$ and $c = 8.20 \text{ \AA}$ (Sawaguchi et al(41)). The X ray study of Sawaguchi et al(41) revealed that the structure of the orthorhombic phase is derived from the cubic perovskite-type lattice essentially through antiparallel displacements of Pb ions along one of the original $\langle 110 \rangle$ directions, which is called the a axis. A subsequent detailed investigation of this structure by Jona et al(42), on the basis of X ray diffraction photographs of single crystals and neutron diffraction pattern of polycrystalline material has revealed that the oxygen ions are displaced antiparallel to each other in the (001) plane. They also found the existence of some uncompensated oxygen displacements along the $[001]$ axis. As a consequence of these displacements the $[001]$ axis is polar and hence this phase should exhibit piezoelectric effect, in accordance with the results of Roberts(43).

In the light of the fact that no evidence of ferroelectricity (e.g., hysteresis) could be found in ceramics, Jona et al(42) concluded that the polarisation along the C axis due to the uncompensated oxygen displacements, was not easily switchable, if at all, because of the strong distortion of the oxygen octahedra caused by the antiparallel displacements in the (001) plane.

Further, the application of an electric field lowered the Curie temperature, and in the vicinity of the transition temperature double hysteresis loops were observed, due to the inducing of a ferroelectric (Rhombohedral) phase by the applied field (Shirane(5)). Thus summing up, pure Lead Zirconate is primarily antiferroelectric, it does not display evidence of strong polarity and pyroelectric and piezoelectric effects are small.

Sawaguchi(44) showed that substitution of about 3 atomic percent Ti^{4+} for Zr^{4+} in antiferroelectric Lead Zirconate brings about a ferroelectric phase in a narrow temperature range. This range is extended by substitution of more Ti^{4+} until, with an addition of 5 or 6 at %, the ferroelectric phase persists from room temperature to the Curie point. Jaffe(45) found that the antiferroelectric

$Pb(ZrSn)O_3$ compositions may also be modified by Ti^{4+} substitution for $(Zr,Sn)^{4+}$, and that in this case the temperature interval in which the ferroelectric and antiferroelectric states are of nearly equal energy is markedly wider than in compositions not containing Sn^{4+} .

It has been shown that the substitution of substantial amounts of Ti^{4+} for Zr^{4+} (Sawaguchi(44)), Ba^{2+} for Pb^{2+} (Shirane et al(46)), or Nb^{5+} for Zr^{4+} (Berlin court et al(47)) brings about a ferroelectric rhombohedral phase. The substitution of Sn^{4+} for $(Zr,Ti)^{4+}$ in

$\text{Pb}(\text{Zr},\text{Ti})\text{O}_3$ lowers the distortion of the ferroelectric rhombohedral phase and reduces the volume difference between the ferroelectric and antiferroelectric phases (Jaffe et al(48)). Nb^{5+} as an excess-valency substituent for Zr^{4+} increases the volume resistivity and generally reduces the coercive electric fields (Jaffe(49)).

The stability of phases in modified Lead Zirconate system was studied in detail by Berlincourt and his coworkers(Berlincourt et al(50)). They studied the phase diagram of the system

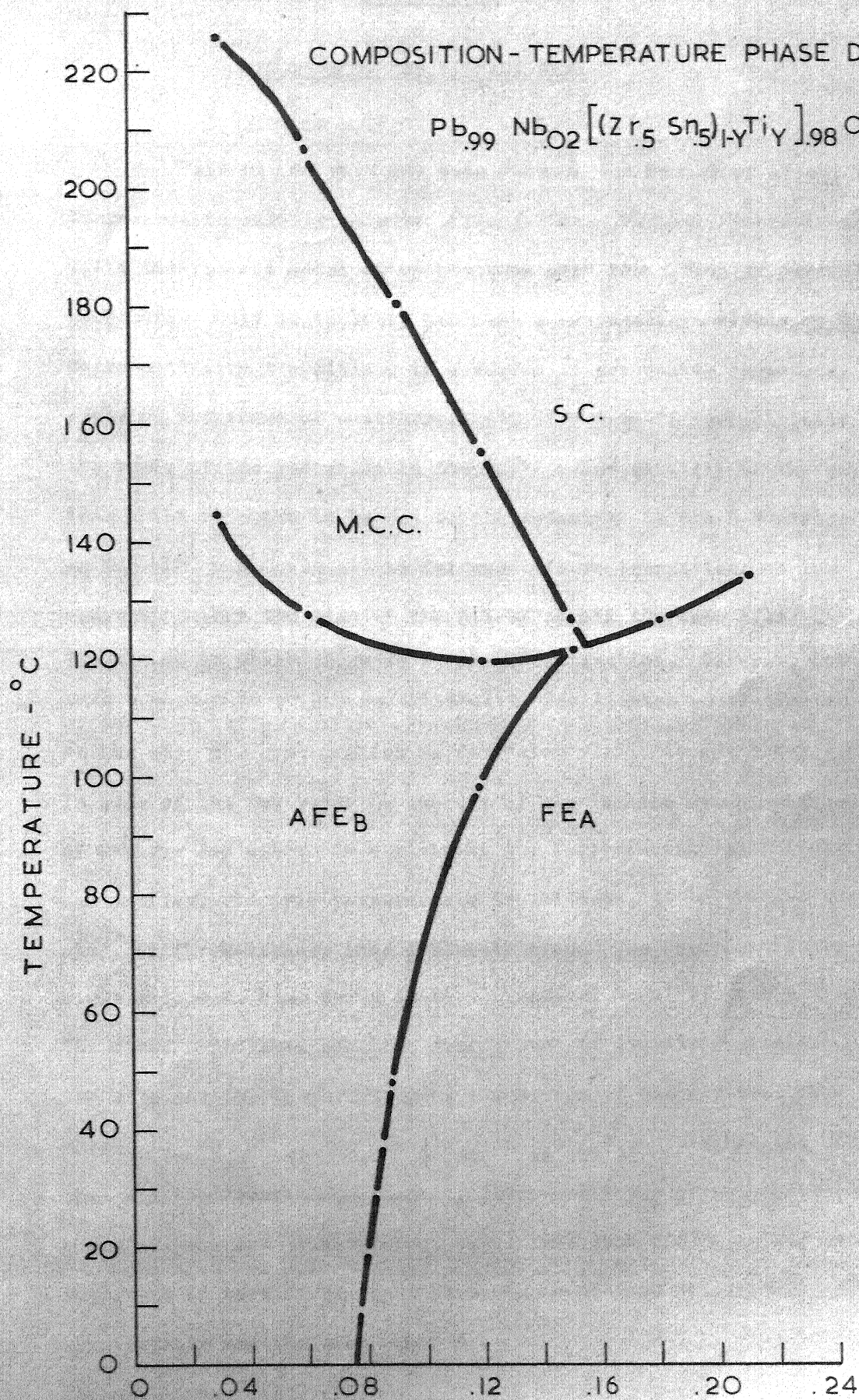
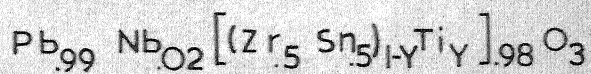


for $z = 0.01$ and 0.02 , $y = 0.0$ to 0.1 and $x = 0.0$ to 0.5 .

These phase diagrams were determined from the plots of dielectric constants, thermal expansion and remanent polarisation as functions of temperature. They also studied the pressure enforced ferroelectric-antiferroelectric transition with and without different biasing fields for many compositions in these systems.

These phase diagrams differ slightly for increasing and decreasing temperature. This is because of the fact that the transition from the ferroelectric to antiferroelectric phase and vice versa depends upon the free energy difference between the two phases and hence sometimes poling might be required to get back the ferroelectric phase if the transition while cooling is from antiferro to ferroelectric phase. A typical phase diagram for $\text{Pb}_{.99}\text{Nb}_{.02} ((\text{Zr}_{.5}\text{Sn}_{.5})_{1-y} \text{Ti}_y)_{.98} \text{O}_3$ is as shown in Fig. 2, for increasing temperature.

COMPOSITION - TEMPERATURE PHASE DIAGRAM.



CHAPTER - IV

PURPOSE OF THE PRESENT WORK

Till now no work has been done on the Mossbauer effect in ferroelectric-antiferroelectric transition. Further, there is no valid theoretical model which predicts such transition in perovskite compounds. Only Krainik(51) has made a systematic analysis of the ferro-antiferro transitions in a series of perovskite compounds. He explains the onset of antiferroelectricity from ferroelectricity on the basis of the reduction in the ionic polarizability of the oxygen ions which is shown to be due to the reduction in the B-O distance in the ABO_3 compounds at the ferro-antiferro transition, on the assumption that the size of the B ions remain the same after the transition in which there is a volume contraction. However, how far such a change in oxygen polarizability facilitates antiferroelectricity rather than the continuation of ferroelectricity is not clear. Further, in view of the far reaching success of the lattice dynamical theory of Cochran and others in explaining the ferroelectric-paraelectric and antiferroelectric-paraelectric transitions, it is thought that a study of the Mossbauer line intensity around the ferro-antiferro transition might give some clue for a lattice dynamical model of such a transition. The other objectives are, the measurement of the field gradient at the tin site and the Isomer Shift as a function of temperature. The compound chosen is $Pb_{.99}Nb_{.02}((Zr_{.5}Sn_{.5})_{.88}Ti_{.12})_{.98}O_3$. This has the advantage that all the transitions, namely, ferro-antiferro-paraelectric occur at comparatively low temperatures, i.e., less than 125° C. This is quite important in view of the fact that the recoilless fraction for Sn^{119} is considerably smaller than for Fe^{57} .

CHAPTER - V

EXPERIMENTAL

5.1 SAMPLE PREPARATION

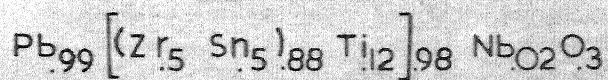
The sample used in the present study was kindly supplied by the Clevite Corporation, U.S.A. It was prepared in the following way. The various constituents, namely, PbO , ZrO_2 , SnO_2 , TiO_2 and Nb_2O_5 were taken as per formula weight and drymixed. They were then mixed thoroughly under acetone and homogenised at 900°C for three hours. The homogenised sample was again pulverised and mixed thoroughly under acetone. Then it was sintered at 1300°C for two hours in PbZrO_3 atmosphere, to take care of the loss of PbO because of its high volatility, in the form of pellets of 12 mm dia. and 1 mm thickness.

The X ray diffraction pattern of the supplied sample showed extinctions characteristic of a rhombohedral lattice. No detailed study for the determination of the accurate cell parameters was made, as it was not necessary in the present study, in the absence of the knowledge of the accurate position of the various ions constituting the lattice.

5.2 THERMAL EXPANSION MEASUREMENTS

Fig. 3 is the reported thermal expansion data of Berlincourt(50). It is reproduced here just to emphasize that for the particular composition, used in the present study, the low temperature, ferro-antiferro, transition is a reversible one. As might be expected, there is a volume contraction at the ferro-antiferro transition and volume expansion at the antiferro-paraelectric transition.

LINEAR THERMAL EXPANSION OF



(UNPOLED SAMPLE)

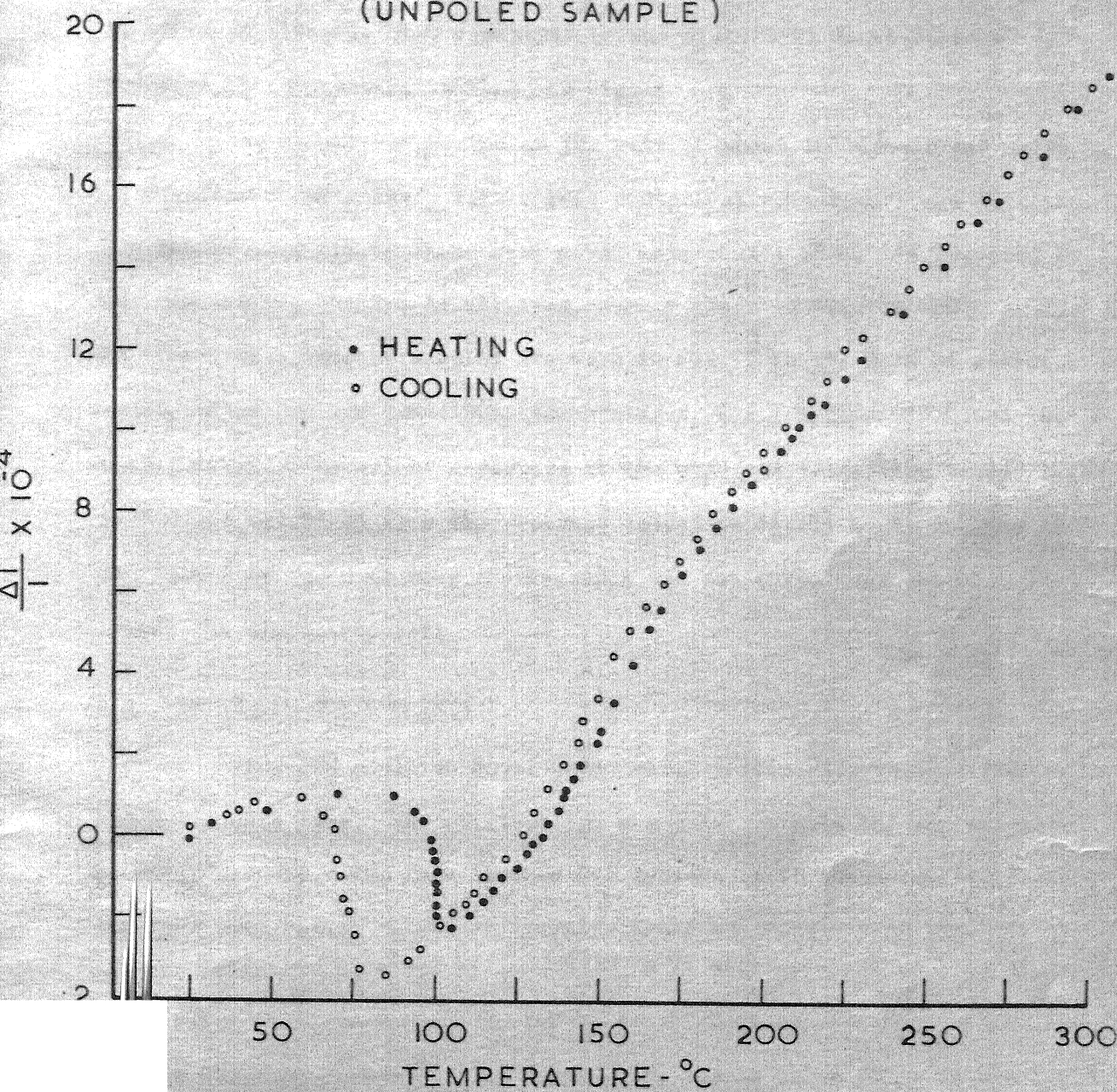


FIG.3.

5.3 DIELECTRIC MEASUREMENTS

The dielectric measurements were made with silver electroded pellets, using a General Radio Type 716-C capacitance bridge, at 1 Kc/sec. The values of the dielectric constant at various temperatures is given in Table 1. The variation of the dielectric constant as a function of temperature is shown in Fig. 4.

The sample was heated at the rate of about 10° C/hour and using an Electromax controller, fairly good control of temperature was obtained. The temperature fluctuations were never more than $\pm 1^\circ$ C. As reported by Berlincourt(50) the two transitions, namely, ferro-antiferro and antiferro-para (multiple cell) are seen in Fig. 4 in the form of dielectric anomalies at the two transition temperatures, i.e., around 95° C and 120° C respectively. The slight departure in the observed transition temperatures (97° C and 121.5° C) from the reported values is likely to be because of the fact that our measuring thermocouple was not quite near the sample inside the dielectric cell.

5.4 HYSTERESIS MEASUREMENTS

Using the modified Sawyer-Tower circuit (Fig. 1), we observed the hysteresis loop. The oscilloscope was calibrated in the way suggested by E.A. Sack(52). The room temperature hysteresis is shown in Fig. 5. The room temperature values of coercive field and spontaneous polarisation are respectively $E_c = 5.0$ KV/cm and $P_s = 27$ micro-coulomb/cm². They agree fairly well with the reported values of Berlincourt ($E_c \approx 5$ KV/cm and $P_s = 26$ micro-coulomb/cm²). On heating the sample above 95° C double loops were observed in the antiferroelectric region (Fig. 5). On cooling the sample back to room temperature, the original single hysteresis loop was observed thereby confirming once again that the first transition is a reversible one.

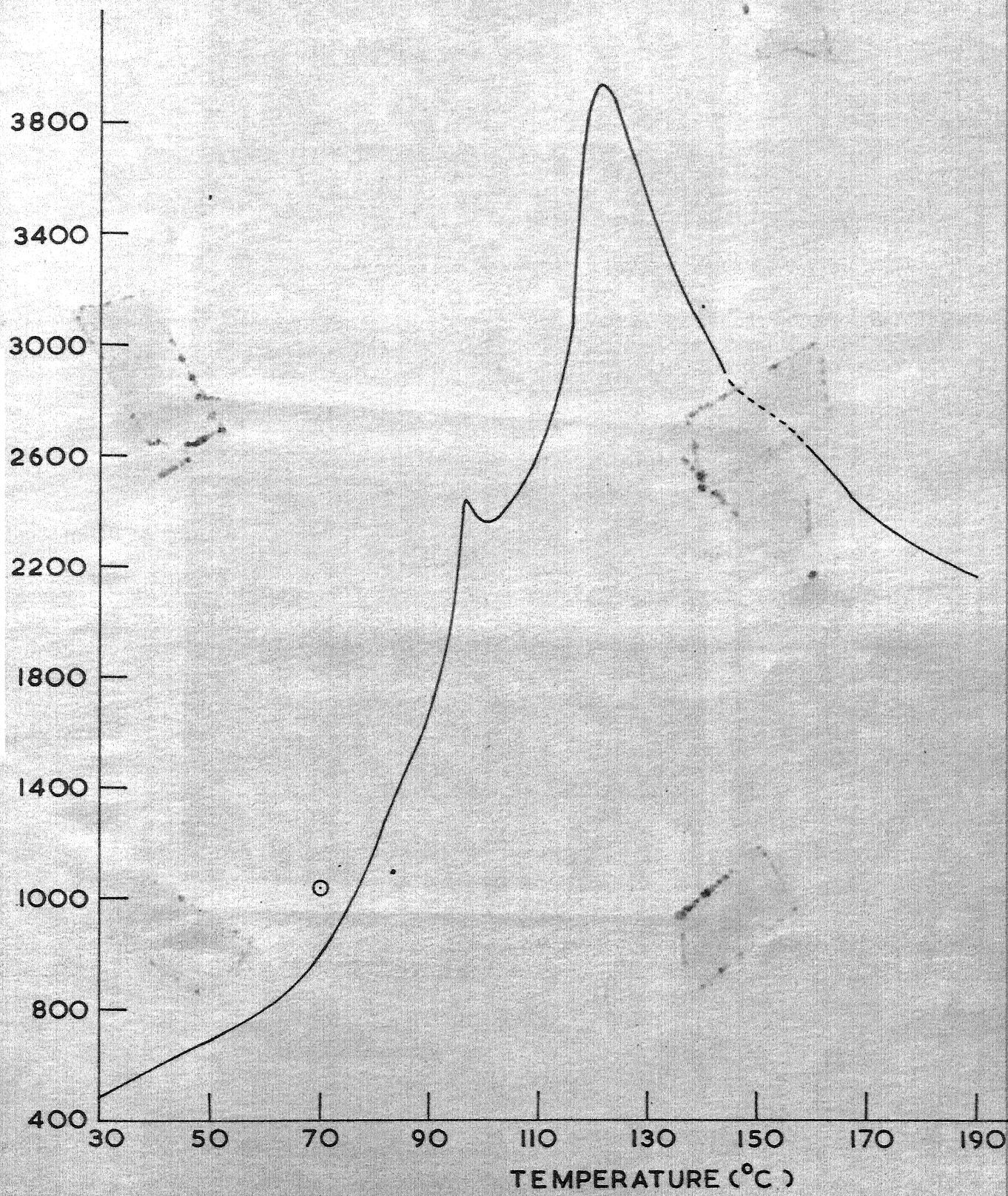


FIG.4

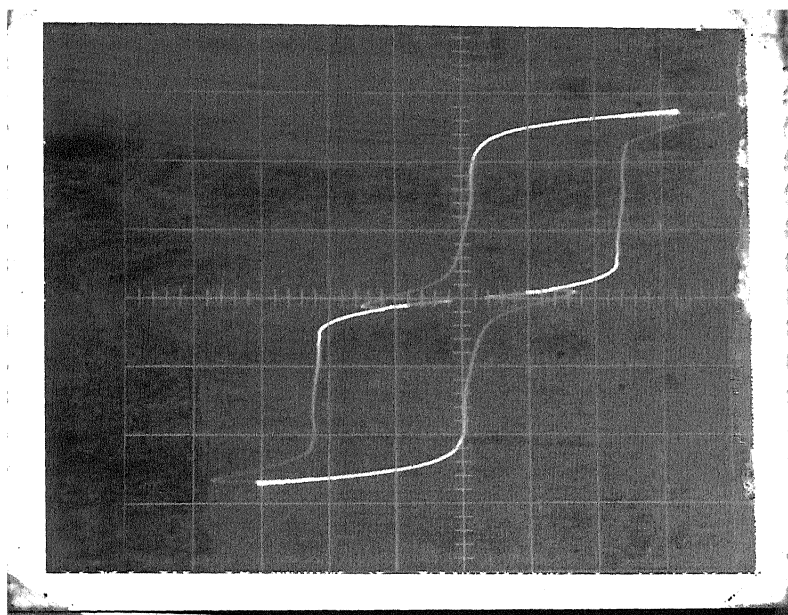
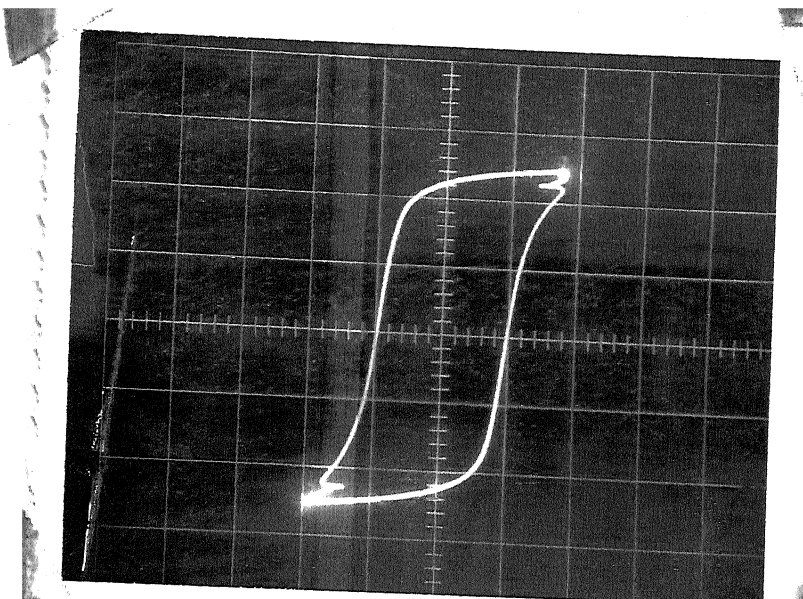


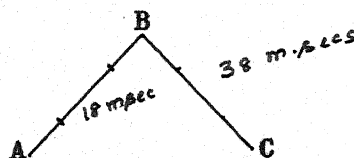
FIG. 5

FERROELECTRIC-ANTIFERROELECTRIC
HYSTERESIS LOOPS

5.5 MOSSBAUER EFFECT MEASUREMENTS

The Mossbauer effect measurements in the powdered sample were carried out using a constant velocity, loud-speaker driven unit. A simple block diagram of the set up is shown in Fig. 6.

By changing the amplitude of the triangular pulses from the frequency generator with a potentiometer device, the frequency of vibration of the loud-speaker diaphragm and hence the velocity of the source attached to this diaphragm is changed. The synchronous pulse emitted every one cycle from the frequency generator is utilised in providing the necessary delay timings to the Gate circuit, so that only for a part of the positive and negative motion of the waves, counts are registered. This is essential to take care of any slight deviation of the pulses from being strictly triangular. For the present study, the frequency used was 13 cycles/sec and hence the width of the positive and negative regions is 38 milliseconds each, as shown in Fig. given below.



In this case only for about 18 milliseconds in each region the counts were registered.

The velocity scale was first calibrated by using a Fe^{57} source and a Fe^{57} enriched iron foil absorber. The source used in the present study was Sn^{119} in palladium. The 'f' factor for this source is 0.4 and the half width observed with tin foil absorber was about 1.0 mm/sec.

The sample was sandwiched between two Be foils using two cooper blocks, the dimensions of which are shown in Fig. 7. The thickness of

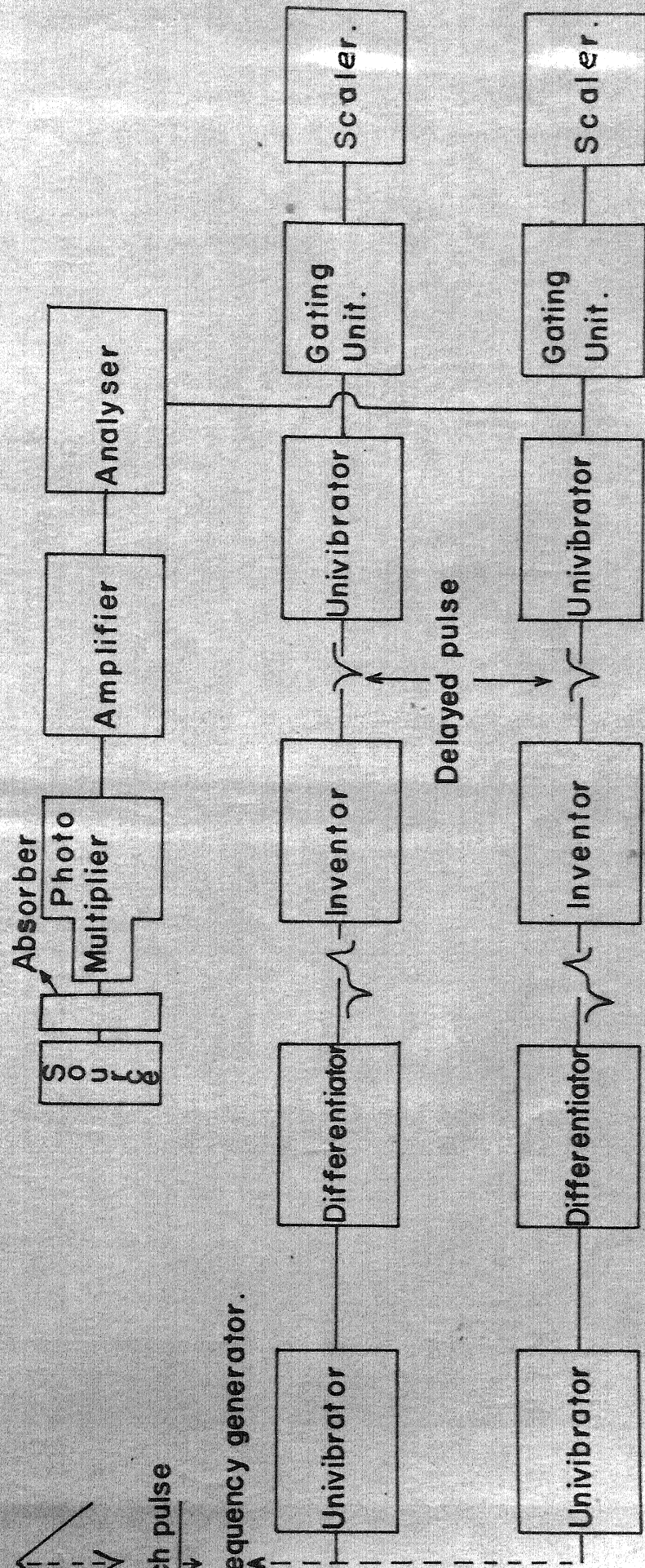
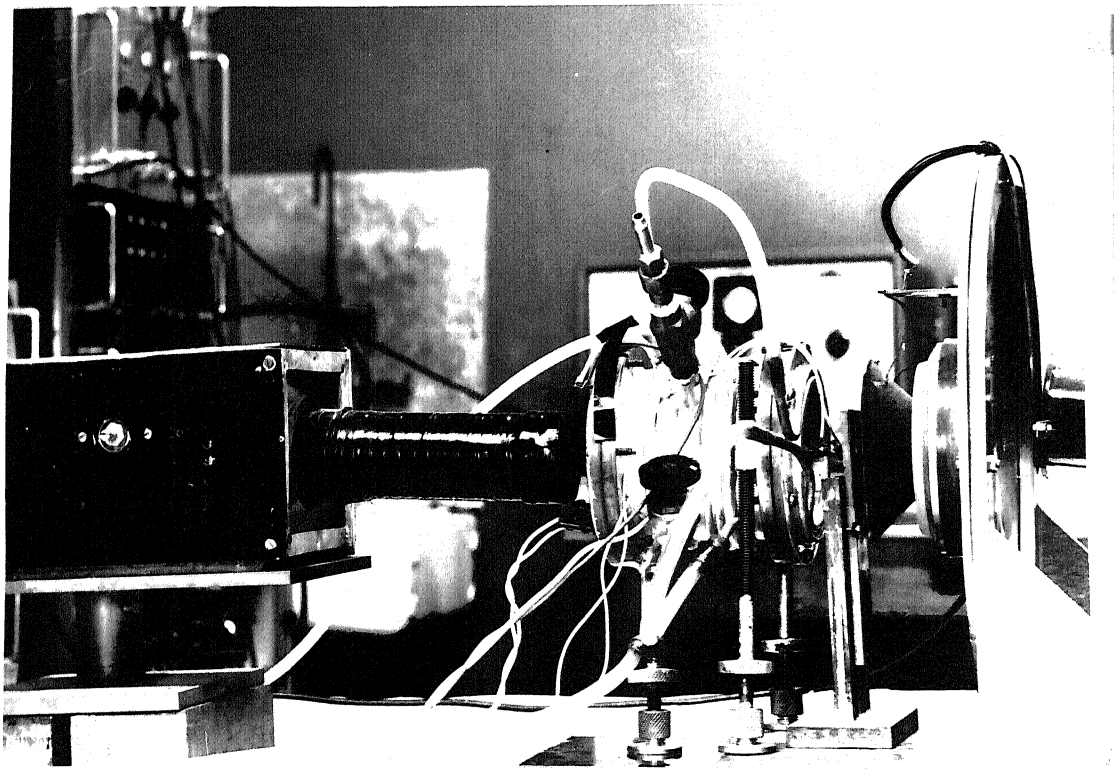
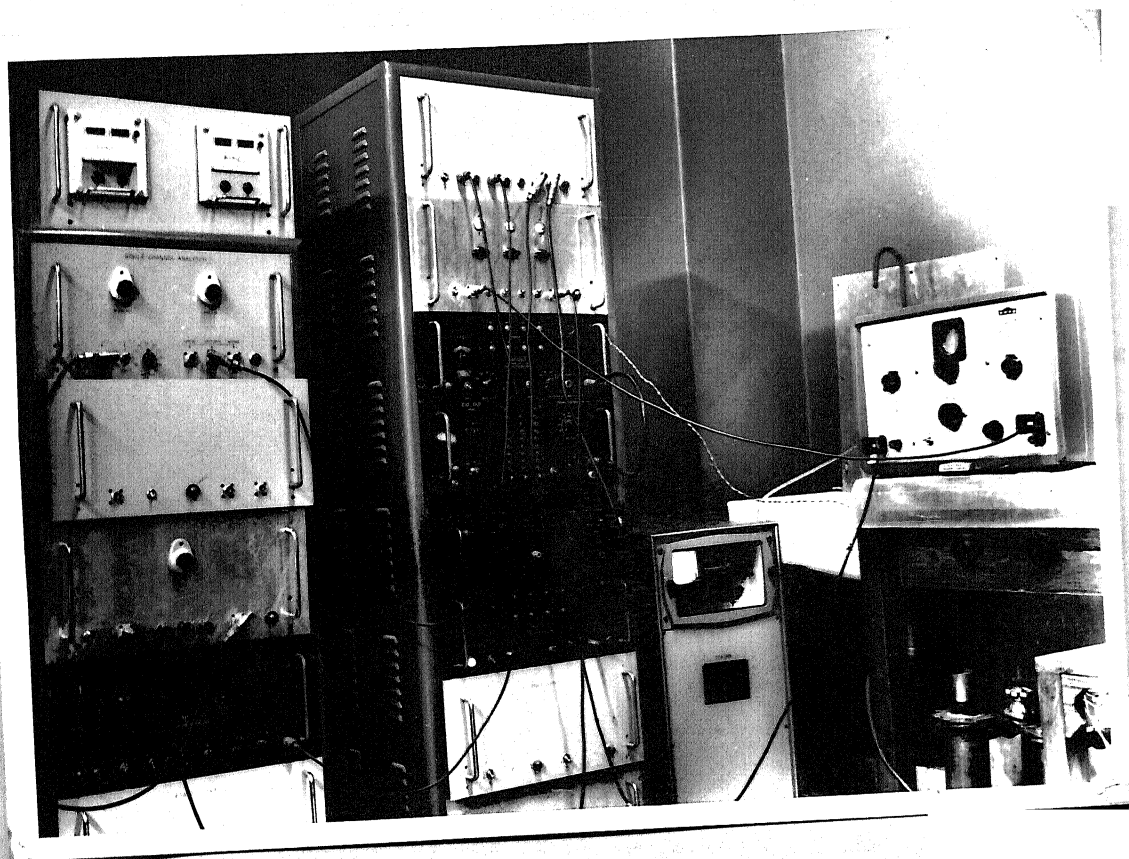


FIG.6. Block diagram of the mossbauer setup.



the absorber used was about 0.005 inches. During each run of the spectrum, at each velocity (both positive and negative) counts were registered for 5 minutes.

5.5.1 Furnace Assembly

Though the sample had just to be heated in ambient atmosphere to study the Mossbauer effect as a function of temperature, to facilitate multipurpose use in future, a vacuum furnace was designed and fabricated. The design of the furnace with the sample holder is shown in Fig. 7. The winding material used was Kanthol D and the total resistance of the wire used was about 40 ohms. As the winding space available on the muffle was only 3", it was made into a coil of 1/8" dia. and the resulting coil was wound. To prevent shorting, the cementing material used was alundum. Two thermocouples, one for controlling the temperature and the other for measuring the exact temperature of the specimen were provided as in Fig. 7. For better temperature control the control thermocouple was placed just outside the furnace coil. For one full scan of +5 mm/sec. to -5 mm/sec., which took about 6 hours, with an Electromax controller and a 100 watt bulb in series with the furnace, temperature fluctuation was never more than $\pm 1^{\circ}$ C. Two stainless steel radiation shields were provided to minimize the radiation losses (Fig. 7). The temperature gradient along the furnace, around its centre, was less than a deg. Cent. over a region of about $\frac{1}{2}$ ". Cooling coils were provided over the body of the furnace and the two end flanges to protect the source, which was quite close to one of the Be windows, from getting heated up. The system was tested for leakage with a Helium Leak Detector and was found to give a vacuum of about 30 microns with just a mechanical pump.

VACUUM FURNACE ASSEMBLY

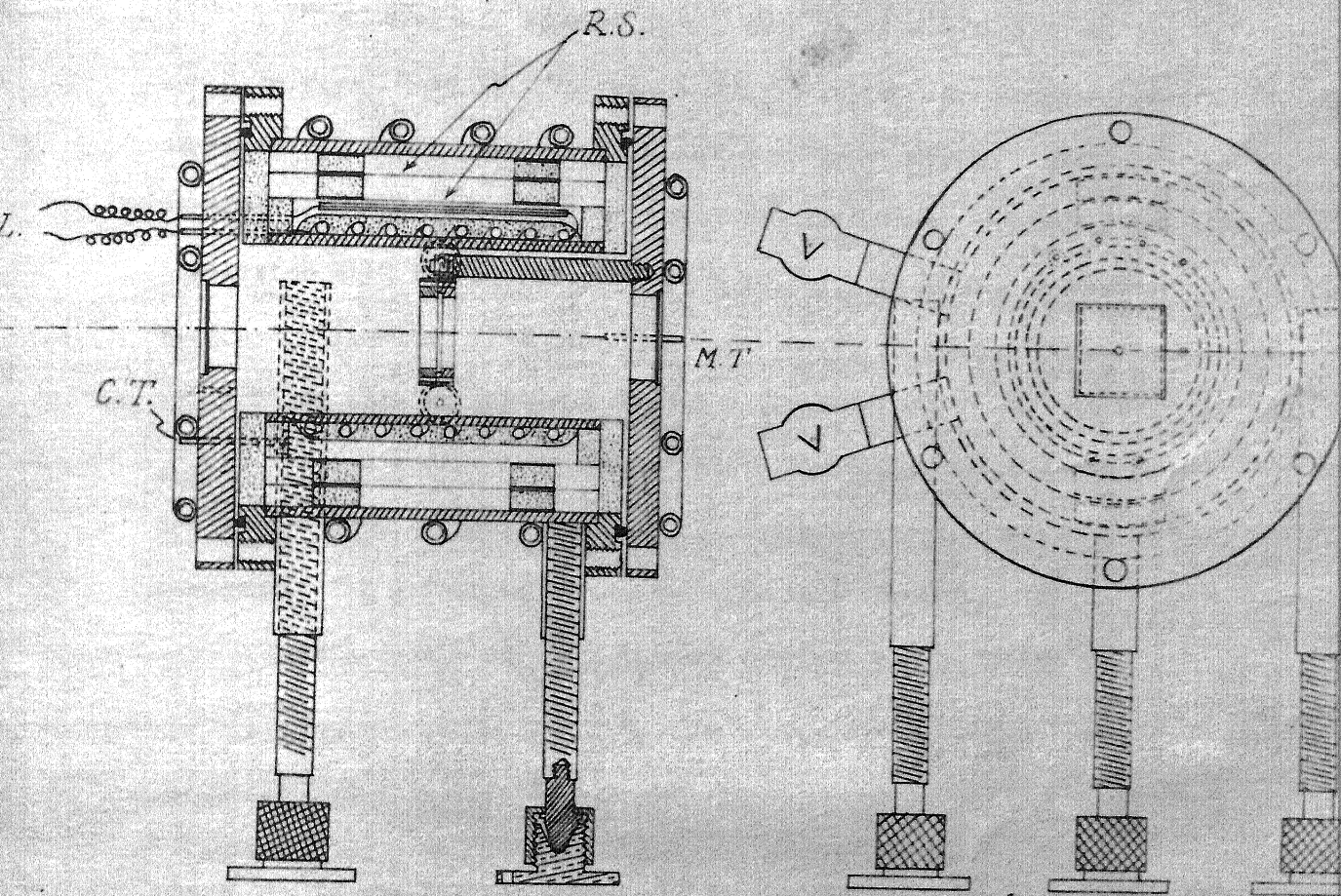
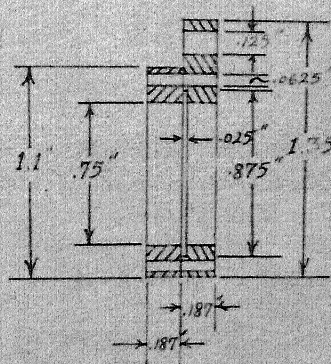


FIG. 7

P.L.: POWER LEADS
 C.T.: CONTROL THERMOCOUPLE
 M.T.: MEASURING THERMOCOUPLE
 R.S.: RADIATION SHIELD



SAMPLE HOLDER

5.5.2 Curve Fitting

The Mossbauer spectra obtained at various temperatures are shown in Figs. 8 to 13. To reduce the scattering each run was repeated at least six times. In spite of many runs some amount of scattering would always be there due to the voltage fluctuation or other fluctuations associated with the electronics of the set up. So to get reasonably accurate parameters from the experimental spectrum, a least square analysis of each set of experimental data was carried out.

The computer programme suggested by Rhodes et al(53) for use in CDC 3600 computer was suitably modified for use in IBM 7044 computer. The principle of the analysis is as follows.

We assume that the Mossbauer spectrum can be fitted to

$$y = \sum_{j=1}^N \left(\frac{A_j}{1 + \frac{(x - C'_j)^2}{B'_j}} \right) + F + Gx + Hx^2 \quad (5.1)$$

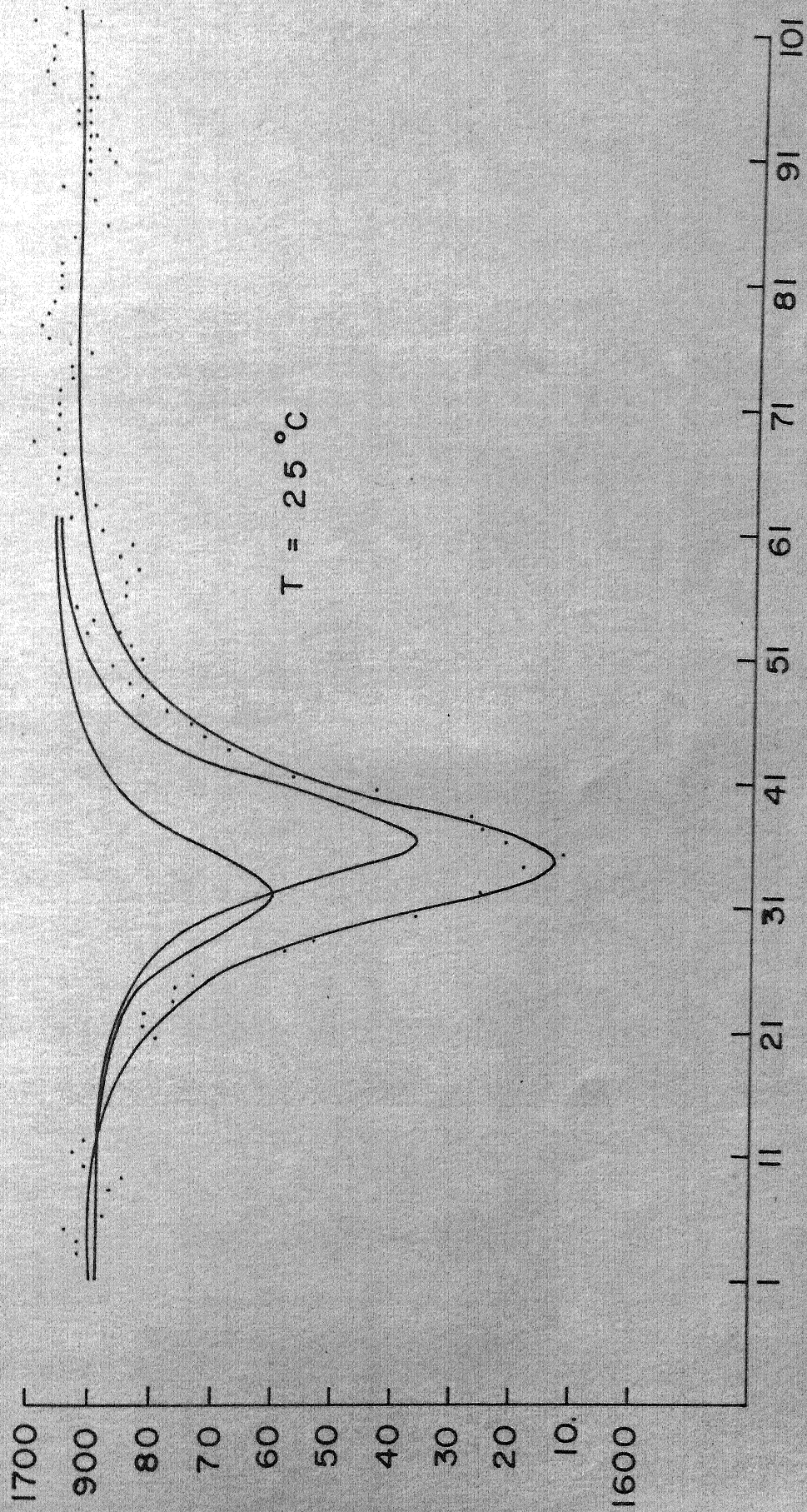
where x is the channel number, N is the number of Lorentzian shapes with peaks at C'_j , heights A_j and B'_j is the square of the half width at half maximum. To take care of the deviation from the strictly Lorentzian variation at the wings of the spectrum, the nonlinear term $F + Gx + Hx^2$ is introduced.

It is assumed that

$$C'_j = C_j + \gamma_j \quad \text{where } C_j \gg \gamma_j \quad (5.2)$$

and

$$B'_j = B_j + \beta_j \quad \text{where } B_j \gg \beta_j \quad (5.3)$$



CHANNEL NUMBER

FIG. 8

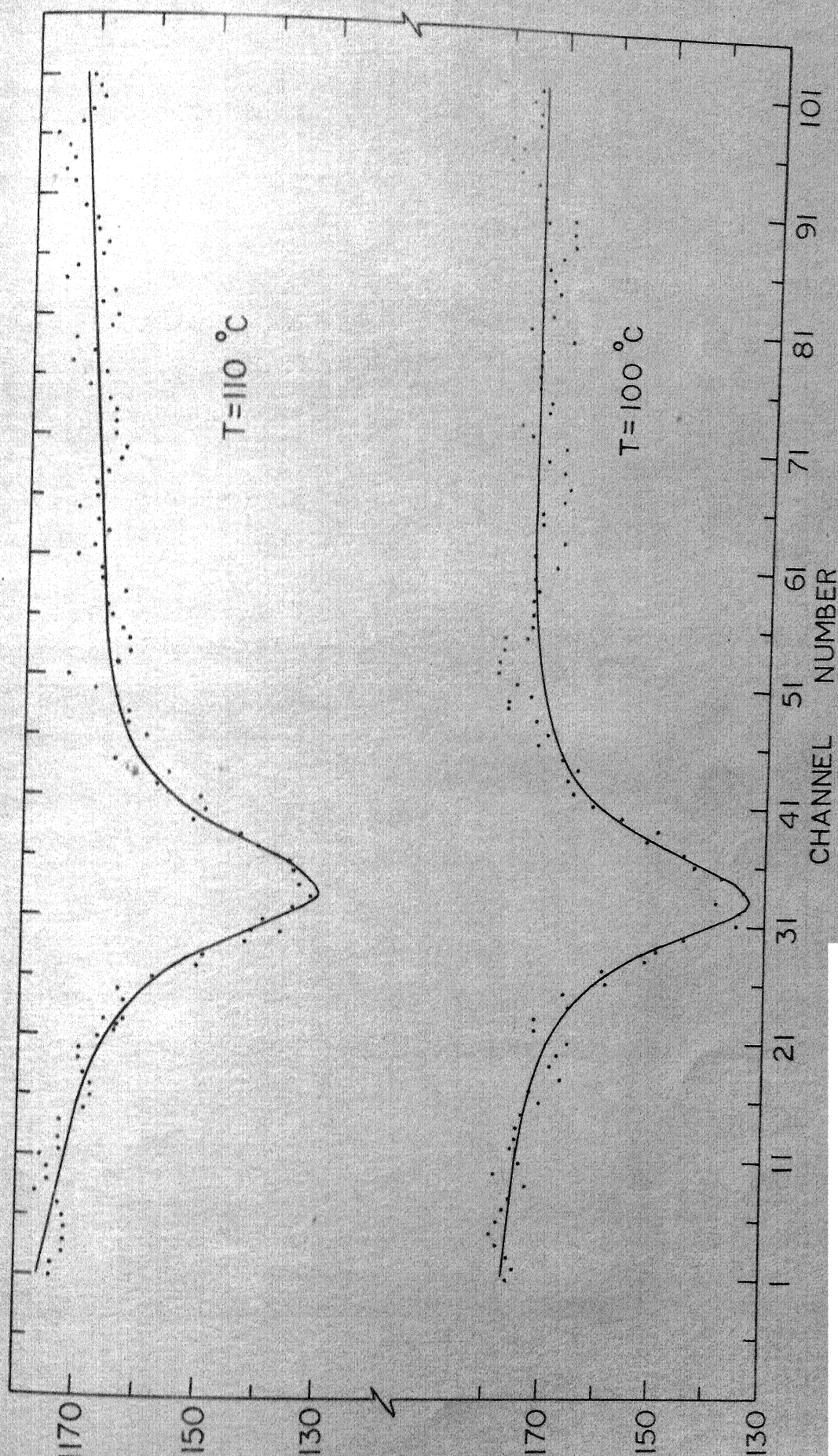


FIG. 11

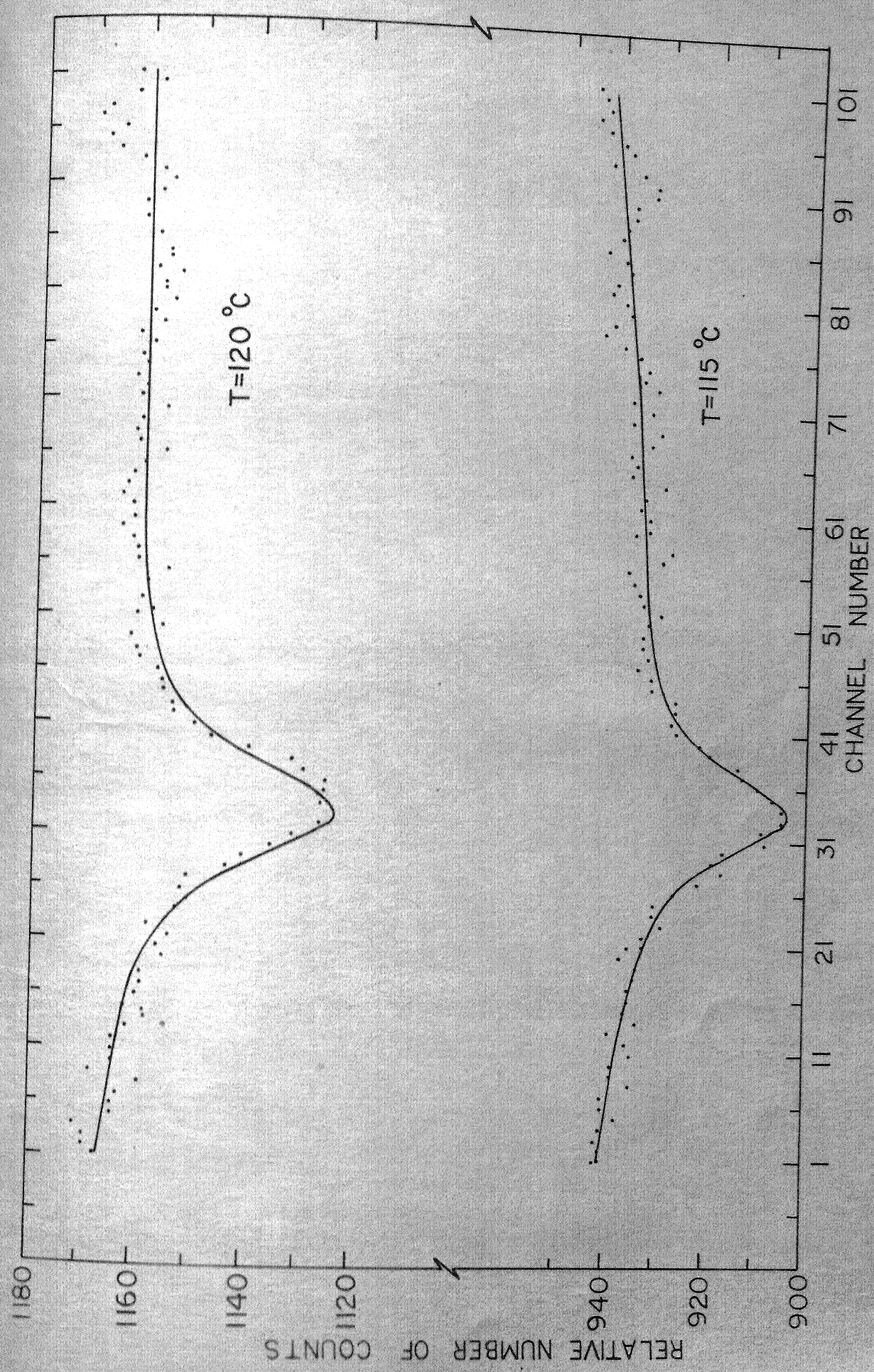
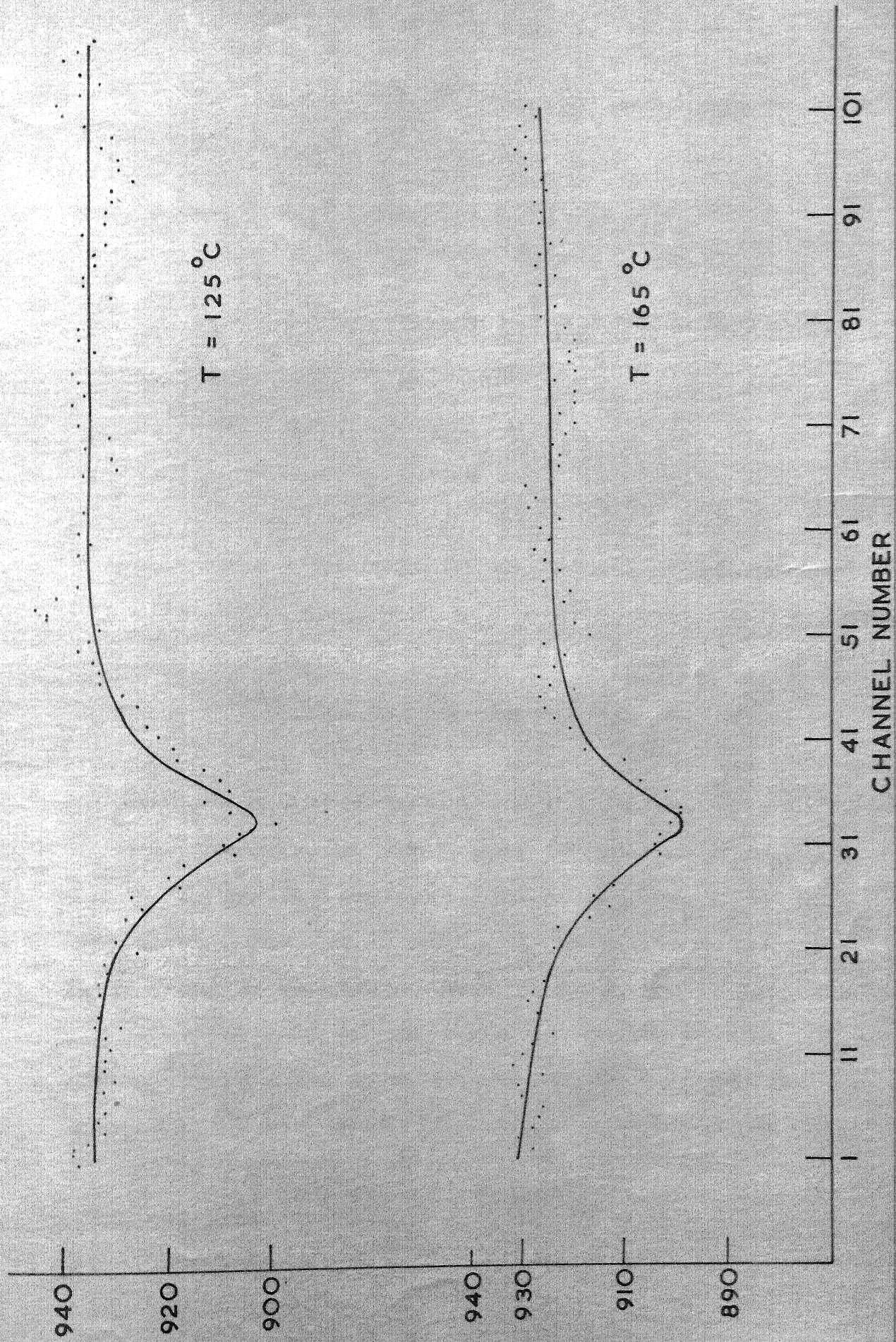


FIG.12



Substituting eqns. (5.2) and (5.3) in eqn. (5.1) and keeping only the first order terms in γ_j and β_j ,

$$y \approx \sum_j \frac{A_j}{1 + B_j(x-C_j)^2 + \beta_j(x-C_j)^2 - 2\gamma_j B_j(x-C_j)} + F + Gx + Hx^2 \quad (5.4)$$

Expanding (5.4) in a Taylor series about $\gamma = \beta = 0$ to first order, and defining the parameters D_j etc. as,

$$D_j = 2A_j \gamma_j B_j; \quad E_j = -A_j \beta_j$$

$$P_{ij} = x_i - C_j \quad \text{and} \quad q_{ij} = 1 + B_j(x_i - C_j)^2$$

we find, to obtain a least square fit, that the following equation should be a minimum, i.e.,

$$S = \sum_i \left(y_i - \sum_j \left(\frac{A_j}{q_{ij}} + \frac{D_j P_{ij}}{q_{ij}^2} + \frac{E_j P_{ij}^2}{q_{ij}^2} \right) - F - Gx_i - Hx_i^2 \right)^2 \quad \dots (5.5)$$

The constraints in (5.5) for the minimum of (5.5), namely, $\frac{\partial S}{\partial A_j} = \text{etc} = 0$ yield $3n+3$ linear equation in $3n+3$ unknown fit parameters A_j, D_j, E_j, F, G and H . The above $3n+3$ equations are then solved for A_j, D_j etc. by Gauss method. From the A_j, D_j and E_j, β_j and γ_j are obtained. Inserting these in eqn. (5.4) the new C_j 's and B_j 's are $C_j(\text{new}) = C_j(\text{old}) + \gamma_j$ etc. The procedure is repeated for a new solution. This iteration may be continued until the desired accuracy is obtained. The error analysis of the various parameters is done in the usual way.

CHAPTER - VI

RESULTS AND DISCUSSIONS

6.1 QUADRUPOLE SPLITTING

The room temperature spectrum is given in Fig. 8. The observed width for a single line spectrum was considerably larger than the natural line width observed for the geometry of the present set up. The line broadening in this case can be due to the following reasons; (a) due to the superimposition of the unresolved quadrupole partners, which should be observed for the present case since the symmetry of the lattice is lower than cubic, and, or, (b) because of the cationic vacancies introduced due to the presence of Nb^{5+} ions. The effect of cation vacancies in KCl has been studied by DeCoster et al(54). As per their observation, because of the interaction between the cation vacancy and the Mossbauer ion, a quadrupole splitting or a line broadening if the quadrupole partners are not resolvable would result. In such a case the splitting or the broadening would be temperature independent. The reasoning (b) is more unlikely because of the facts that only about .02 mole % of the Nb^{5+} is doped in the compound and that the line width is not temperature independent. The existance of tin in a lower valence state instead of the quadrivalent state and hence the introduction of anion vacancies is unlikely because the observed Isomer Shifts, referred to the systematics of Kistner et al(27), essentially correspond to the quadrivalent tin. Here again the introduction of anion vacancies would lead to line broadening, in case the quadrupole splitting introduced because of them are not resolvable, and would be

temperature independent as shown by Bhide et al(55) for the case of 1 mole % of Fe in BaTiO_3 absorber.

Thus the reasoning (a) is substantiated by the decrease in the observed line width from $1.28 \text{ mm/sec} \pm .05 \text{ mm/sec}$ at 25°C to about $1.06 \text{ mm/sec} \pm .05 \text{ mm/sec}$ at 95°C , above which it oscillates within a range of $\pm .05 \text{ mm/sec}$ which can be assigned to the statistical deviations inherent in the present measurements. The values of half widths at various temperatures are given in Table 2. The half width in the cubic phase at 165°C is $1.04 \text{ mm/sec} \pm .05 \text{ mm/sec}$ which agrees well with the natural line width observed for the present set up. A least square analysis of the room temperature data showed that the room temperature spectrum is a doublet of unequal intensities, with a separation of about $0.40 \text{ mm/sec} \pm .05 \text{ mm/sec}$. For randomly oriented crystallites, as in the present case when powdered sample was used, one would expect the two quadrupolar lines to be of equal intensity. However, as shown by Goldanskii et al(56) and Kagan(57) the anisotropy of the Lamb-Mossbauer factor in a rhombohedral lattice is bound to introduce changes in the observed line intensities. Hence it is surmised that the observed asymmetry in the line intensities is likely to be due to the reasoning of Goldanskii and others.

Our present observation regarding the resolution of the quadrupole partners in the ferroelectric, perovskite, compound containing tin is at variance with the findings of the Russian workers(38). They argue that because the quadrupole moment of Sn^{119} is about 3 fold smaller than that of Fe^{57} , the splitting ΔE would be reduced by 3 orders of magnitude in the case of Sn^{119} as compared with Fe^{57} for the same field gradient, under the assumption that the antishielding

$q = 1.02 \times 10^{13}$ esu/cm³. Since in the powdered sample poling is ruled out, the sign of q could not be determined. The calculated q value in this case is about twice that in BaTiO₃ (Ref. 32). The room temperature spontaneous polarisation ($P_s = 27$ micro-coulomb/cm²) measured in the polycrystalline sample is about the same as that found in BaTiO₃ single crystals ($P_s = 26$ micro-coulomb/cm²). Since the porosity in the ceramic specimens lowers the measured P_s values to a great extent, it may be concluded that the P_s value in the single crystal of the present compound would be considerably greater than that in BaTiO₃ single crystal. Thus the result that the present q value is about twice that in BaTiO₃ is interesting in the light of the observation that ΔE follows closely the variation of P_s^2 with temperature in BaTiO₃, by Bhide et al(32).

In the high temperature runs since the absorption and quadrupole splitting decrease the theoretical resolution could not be carried out.

6.2 ISOMER SHIFT

The Isomer Shift for the room temperature spectrum relative to white tin was found to be -2.65 mm/sec \pm $.05$ mm/sec. This is quite close to the Isomer Shift of SnF₄ relative to white tin (-2.77 mm/sec). From electronegativity and ionic character correlations, Shirley (59), has come out with a value for the ionicity of SnF₄ as about 85% and that tin is essentially in Sn⁴⁺ state in SnF₄. Shirley's analysis regarding the variation of Isomer Shift with electronegativity and with percentage ionic character (on the basis of Pauling model) (Ref.60) of the binding suggests that the present compound is largely ionic in nature

with an ionicity of about $70 \pm 20\%$. From the systematics of Kistner et al(27) it is again evident that the charge state of the present Mossbauer ion is quadrivalent and that the binding is largely ionic. These results again revalidate the earlier conclusion that the broadened line observed at room temperature may not be due to the association of charge compensating vacancies in the lattice.

The Isomer Shift values at different temperatures are given in Table 2. Since the counts were recorded only at every 0.1 mm/sec the error introduced in the final Isomer Shift values is about $\pm .05$ mm/sec. The volume anomalies at the two transitions are relatively small when compared to the volume anomaly in BaTiO_3 (120° C) transition or in PbZrO_3 (230° C) transition. Under these circumstances, the changes in Isomer Shift associated with these transitions could not be fixed. The general increase in the Isomer Shift in the negative side with temperature is precisely due to the second order Doppler Effect.

6.3 MOSSBAUER LINE INTENSITIES

The Mossbauer line intensities at various temperatures were measured in the following way. The Mossbauer line intensity, assuming a Lorentzian line shape, is given as $\pi \tau_{\frac{1}{2}} I_{\text{max}}$ where $\tau_{\frac{1}{2}}$ is the half width at half maximum and I_{max} is the maximum intensity A_j (eqn. (5.1)). Since the base line for each run is different, the areas calculated directly from the spectra would be in error because of the fact that the value of A_j depends upon the value of the base line for the same percentage of absorption. Hence for each run using eqn. (5.1) the base line was calculated for the final accurate parameters. For all spectra, the individual areas were calculated using the respective A_j 's

corresponding to a base line of 100. The resulting areas were normalised with respect to the area of the room temperature spectrum. The various values of f_T/f_{25} for different temperatures are given in Table 3. Their variation as a function of temperature is depicted in Fig. 14.

It is interesting to note from Fig. 14 that there are anomalous changes in the intensity around the two transition temperatures. As per Dvořák's qualitative treatment, we find an anomalous decrease in the line intensity at the para-antiferroelectric transition at 120° C. However, here the relative intensity anomaly is not that much as in the ferroelectric transition reported earlier (Ref. 32, and 37). Actually as per Dvořák's explanation on the basis of Silverman's model one would expect a relatively larger intensity anomaly in a para-antiferroelectric transition than in a para-ferroelectric transition. However, it should be noted that the Mossbauer ion in this case is Sn^{119} and in the earlier ferroelectric cases (Ref. 32, and 37) was Fe^{57} and that the mass of tin ion is about twice that of iron. Hence during the excitation of the whole branch of the anomalous mode in a para-antiferroelectric transition, it is quite likely that the reaction of the heavier ions would be relatively smaller than that of smaller ions, which means that the relative changes in intensity of the Mossbauer line around such transitions would depend on the characteristics of the probing ion used. It may be mentioned here that the observed relative anomaly in $f_T/f_{\text{room temp.}}$ for the tin doped BaTiO_3 case, around the transition temperature, compared to that Fe^{57} doped BaTiO_3 (Ref. 36) is in line with the above arguments.

The observation of an anomaly in $F f_T/f_{25}$ at the ferro-antiferroelectric transition evokes new interest for future work. In the absence of a lattice dynamical model explaining such a transition we can make only the following qualitative statement. The short wave part of the transverse

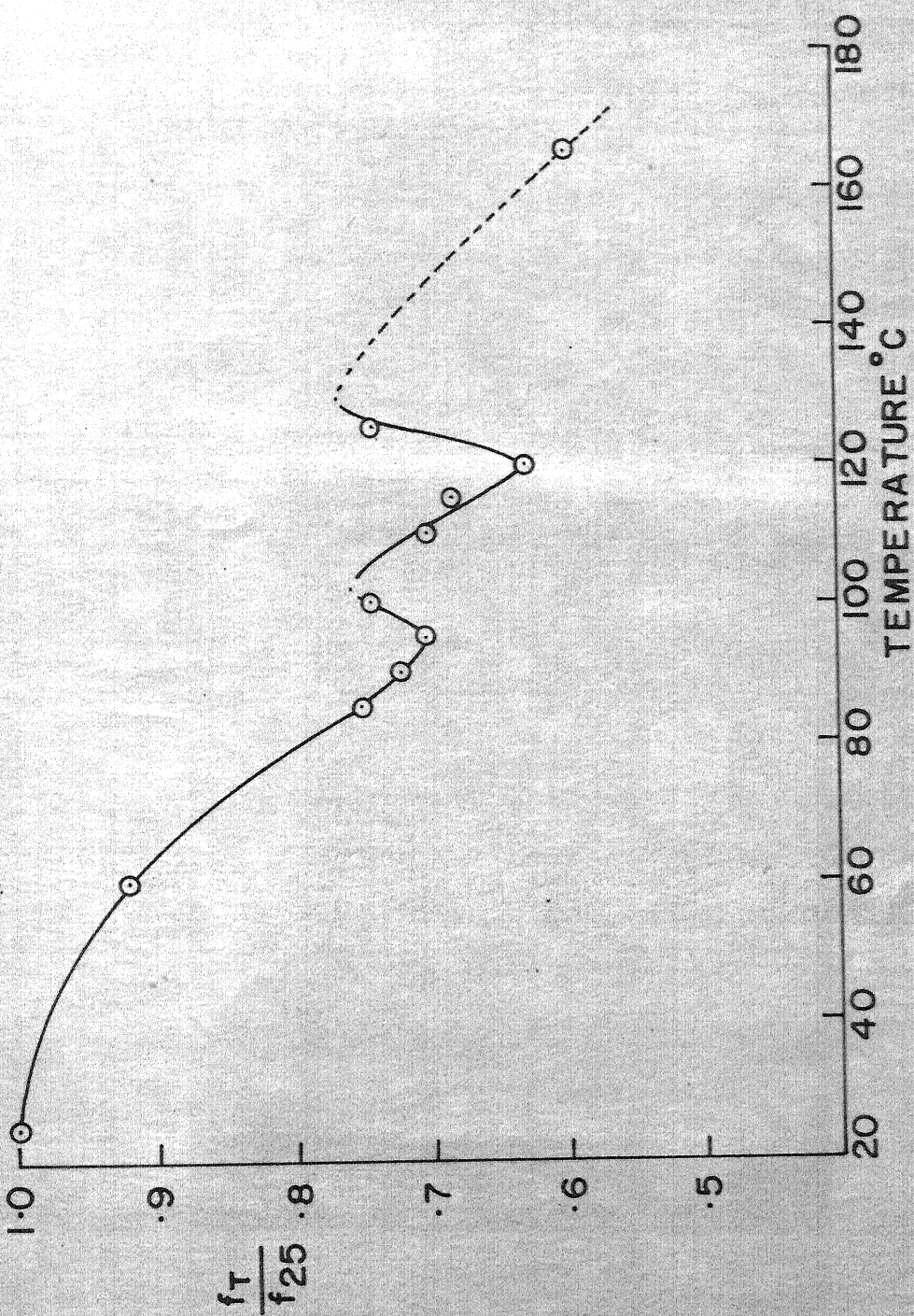


FIG. 14.

optical modes in the materials which exhibit ferro-antiferroelectric transition might be strongly temperature dependent because of the long range coulomb interactions. During the ferro-antiferroelectric transition these modes might be excited and hence lead to an anomalous decrease in the Mossbauer line intensity. To get the exact nature of the changes taking place around the transition, it is necessary to derive an exact model which would predict such a transition, which is beyond the scope of the present work.

Thus we may conclude that our observations are in concurrence with the Silverman model of antiferroelectricity, and that further studies in Fe^{57} and Sn^{119} containing simple perovskites exhibiting the ferro-antiferroelectric transition would pave the way for an exact lattice dynamical approach to such transitions.

TABLE 1**VALUES OF DIELECTRIC CONSTANT AT DIFFERENT TEMPERATURES**

Temperature in °C	Dielectric Constant	Temperature in °C	Dielectric Constant
30	481	102	2384
44.5	617	103	2394
54	705.3	104	2432
64	819.4	109.5	2575
67	922.6	114.5	2938
74	1052	115.5	3240
80	1234	116.5	3410
84	1418	118.5	3829
87	1516	121.5	3965
88.5	1603	122	3953
91	1763	123	3934
92	1926	124	3896
93	1976	125	3836
93.5	2107	126	3758
95	2247	137	3166
97	2454	140	3161
98	2413	146	2845
99	2384	155	2748
100	2373	170	2424
101	2371	190	2175

TABLE 2

ISOMER SHIFT AND HALF WIDTH VALUES AT DIFFERENT
TEMPERATURES

Temperature in °C	Isomer Shift in mm/sec \pm .05 mm/sec (relative to white tin)	Half Width in mm/sec \pm .05 mm/sec
25	-2.65	1.28
60	-2.69	1.20
85	-2.73	1.12
90	-2.67	1.07
95	-2.75	1.06
100	-2.78	1.08
110	-2.75	1.07
115	-2.74	1.06
120	-2.79	1.08
125	-2.73	1.06
165	-2.83	1.04

TABLE 3

MOSSBAUER LINE INTENSITY AT DIFFERENT TEMPERATURES (NORMALISED
TO ROOM TEMPERATURE VALUES)

Temperature in °C	f_T/f_{25}
25	1.00
60	0.92
85	0.75
90	0.72
95	0.70
100	0.74
110	0.70
115	0.68
120	0.62
125	0.75
165	0.59

BIBLIOGRAPHY

1. Y. Takagi et al., J. Phys. Soc., Japan, 13, 272 (1958).
2. R. Pepinsky et al., Phys. Rev., 114, 1217 (1959).
3. W. Merz., Progress in Dielectrics, 4, 103 (1954).
4. C. Kittel., Phys. Rev., 82, 729 (1951).
5. G. Shirane, et al., J. Phys. Soc., Japan, 6, 33 (1951).
6. C.B. Sawyer and C.H. Tower, Phys. Rev., 35, 269 (1930).
7. Känzig et al., Helv. Phys. Acta., 24, 343 (1951).
8. L.E. Cross, Phil. Mag. Series 7, 44, 1161 (1953).
9. L. Onsager, J. Am. Chem. Soc., 58, 1486 (1936).
10. S. Triebhasser, I.B.M. J. Research Develop., 2, 212 (1958).
11. A.F. Devonshire, Phil. Mag. (7), 40, 1040 (1949).
12. J.C. Slater, Phys. Rev., 78, 748 (1950).
13. H.D. Megaw, Acta. Cryst., 5, 739 (1952).
14. E.T. Jaynes., Ferroelectricity, Princeton University Press, Princeton, New Jersey (1953).
15. J.R. Tessman et al., Phys. Rev., 92, 890 (1953).
16. M. Born and K. Huang., Dynamical Theory of Crystal Lattices, Oxford University Press (1954).
17. B.G. Dick Jr. and A.W. Overhauser., Phys. Rev., 112, 90 (1958).
18. W. Cochran., Z. Kristallogr., 112, 465 (1959);
Phys. Rev. Letters, 3, 412 (1959);
Phil. Mag. Suppl., 9, 387 (1960);

and
W. Cochran et al., Bull. An. Phys., Soc., 4, 246 (1959).
19. R.H. Lyddane et al., Phys. Rev. 59, 673 (1941).

20. R.A. Cowley, Phys. Rev. Letters, 9, 159 (1962).
21. A.S. Barker et al., Phys. Rev., 125, 1527 (1962).
22. A. Anderson, Bull. Acad. Sci., U.S.S.R., Vol. 24 (1958).
23. B.D. Silverman, Phys. Rev., 128, 638 (1962).
24. P.B. Moon, Proc. Phys. Soc., 63, 1189 (1950).
25. H.J. Lipkin, Ann. Phys., 9, 332 (1960).
26. L.R. Walker et al., Phys. Rev. Letters, 6, 98 (1961).
27. O.C. Kistner et al., Proc. 2nd Conference on Mossbauer Effect, Sacaly, France, 264-276 (1962), Wiley, N.Y.
28. B.P. Dailey et al., J. Chem. Phys., 17, 1782 (1949).
29. R.M. Sternheimer, Phys. Rev., 80, 102 (1950); *ibid* 84, 244(1951).
30. V. Dvořák et al., Phys. Stat. Soli.3, K9 (1963).
31. V. Dvorak, Phys. Stat. Soli., 14, K161 (1966).
32. V.G. Bhide et al., Phys. Rev., 139A, A1983(1965).
33. A.W. Horning et al., J. Phys. Chem. Solids, 10, 1 (1959).
34. A. Nishioka et al., J. Phys. Soc., Japan, 11, 181 (1951).
35. V.A. Bokov et al., Sov. Phys. Solid State, 7, 1521 (1965).
36. V.V. Chekin et al., JETP. Letters, 3, 135 (1966).
37. V.V. Sklyarevskii et al., JETP Leeters, 3, 135 (1966).
38. M.V. Plotnikova et al., Bulln. Acad. Sciences (U.S.S.R.), 31A, 1119 (1968).
39. S. Roberts, J. Am. Ceram. Soc., 33, 63 (1950).
40. G.A. Smolenskii., Zhur. Tekh. Fiz., 20, 137 (1950).
41. E. Sawaguchi et al., J. Phys. Soc., Japan, 6, 333 (1951);
Phys. Rev., 84, 476 (1951);
ibid, Phys. Rev., 83, 1078 (1951).
42. F. Jona et al., Phys. Rev., 105, 849 (1957).
43. S. Roberts, Phys. Rev. 83, 1078 (1951).
44. E..Sawaguchi, J. Phys. Soc., Japan, 8, 615 (1953).
45. B. Jaffe, Inst. Radio Engrs., 49, 1264 (1961).

46. G. Shirane et al., Acta. Crys., 7, 203 (1954).
47. D. Berlincourt et al., Appl. Phys. Letters, 3, 90 (1963).
48. B. Jaffe, et al., J. Res. Nat. Bur. Stand., 55, 239 (1955).
49. H. Jaffe, Proc. Inst. Elec. Engrs., 109B, Suppl. 22, 351 (1961).
50. D. Berlincourt et al., J. Phys. Chem. Solids., 25, 659 (1964).
51. V. Krainik., Bull. Acad. Sci., U.S.S.R., 28, 546 (1964).
52. E.A. Sack, Research Memo.8.,1041-M17, Westinghouse Research Laboratory, Pennsylvania (1956).
53. E. Rhodes et al., NBS. Tech. Note, 404, 105 (1966).
54. M.DeCoster et al., Phys. Letters, 1, 245 (1962).
55. V.G. Bhide et al., Phys. Rev., 149, 289 (1966).
56. V.I. Goldanskii et al., Phys. Letters, 3, 344 (1963).
57. Yu. Kagan, Soviet.Phys. DOKLADY, 6, 881,(1962).
58. R.M. Sternmeiher, Phys. Rev. 152, 266 (1967).
59. D.A. Shirley, Rev. Mod. Phys., 36, 339 (1964).
60. L. Pauling, The Nature of the Chemical Bond (Cornell Univ. Press, Ithaca, 1960).

GENERAL REFERENCES

- 1) F. Jona and G. Shirane, Ferroelectric Crystals, Pergamon Press, N.Y. (1962).
- 2) D. Megan, Ferroelectricity in Crystals, Methuen and Co., Ltd., (1957).
- 3) A.F. Devonshire, "Some Recent Work on Ferroelectrics", Report in Progress in Physics, Vol. 27, 1964.
- 4) S. Triebwasser, "Ferroelectric Materials" in Modern Materials, Vol. 3, Academic Press, Inc., N.Y. (1962).
- 5) G.K. Werthiem, Mössbauer Effect - Principles and Applications, Academic Press Inc., N.Y. (1964).
- 6) H. Fraunfelder, The Mössbauer Effect, W.A. Benjamin Inc., N.Y. (1962)